Project Report No. 101

EXPERIMENTAL STUDY OF WARM WATER FLOW INTO IMPOUNDMENTS
PART I:
FLOW AND HEAT EXCHANGE NEAR A SURFACE OUTLET IN TWO-DIMENSIONAL FLOW

by
Heinz Stefan
and
Frank R. Schiebe

Prepared for
Department of the Interior
Federal Water Pollution Control Administration

December 1968

CONTENTS

EXPERIMENTAL STUDY OF WARM WATER FLOW INTO IMPOUNDMENTS
PART I: FLOW AND HEAT EXCHANGE NEAR A SURFACE OUTLET IN TWO-DIMENSIONAL FLOW

1. Scope of Investigation

The largest single industrial use of water in the United States is for cooling purposes. Large quantities of the resulting warm water are discharged into natural bodies of water. The flow pattern of the warmer water in the colder recipient can be controlled to a certain extent by the outlet design. The following study was undertaken to show some aspects of the flow of warm water into a colder body of water. There is a substantial difference between the flow of cooling water into a flowing stream and into a stagnant impoundment. Only the latter case was considered. The outlet was an open channel discharging the warm water at the water surface of the impoundment. This report presents the results of studies with two-dimensional flow only; the three-dimensional work is described in another report, as noted in the preface.

The flow of warm water from an open channel into a reservoir containing colder and essentially stagnant water was studied in a laboratory flume. The results give some insight into the mass-, momentum-, and heat-exchange processes at surface cooling water outlets into impoundments. The flume experiment is not a true model of any cooling water outlet into an impoundment. It does, however, permit demonstration and close observation of a number of phenomena which are likely to be found under both natural and more complicated conditions.

2. Experimental Facility

A glass-walled channel 6 in. wide, 15 in. deep, and 40 ft long, mounted horizontally, was used. Warm water was discharged horizontally from a channel about 4 ft long. This length was sufficient to produce a fully or nearly fully developed velocity profile at the point of discharge. Warm water discharge and depth at the outlets were variable and could be controlled. The experimental set-up is shown schematically in Fig. 1.

The flow of warm water on top of the cold water could be observed over a distance of 25 ft. Vertical temperature profiles were recorded with a

Thermistor temperature probe and velocities with the aid of a tethered buoyant sphere. The instrumentation has been described in principle in Reference [1]* and in more detail in [2]. The velocity-temperature probe was mounted on a carriage such that measurements could be taken at any distance from the outlet. Measurements were generally taken in the centerline of the flume, and thus maxima of temperature and velocity were recorded. Velocities must drop to zero at channel walls. In a few cases temperatures were also measured across the channel width and were found to be essentially uniform. Only in the immediate vicinity of the wall was a temperature gradient observed. Deflections of the tethered sphere were measured through the glass walls of the flume with the aid of a cathetometer. This method differs slightly from the one described in Reference [1].

3. Number and Range of Parameters Investigated

A survey of all physical parameters which influence the stratified flow of warm water over cold water in two-dimensional flow can be made by writing the equations of motion for steady flow:

$$0 = - u \frac{\partial u}{\partial x} - w \frac{\partial u}{\partial z} - \frac{1}{\rho_o} \frac{\partial p}{\partial x} + \nu_H \nabla^2 u \tag{1}$$

$$0 = - u \frac{\partial w}{\partial x} - w \frac{\partial w}{\partial z} - \frac{1}{\rho_o} \frac{\partial p}{\partial z} + g \frac{\rho}{\rho_o} + \nu_V \nabla^2 w \tag{2}$$

the equation of heat flow:

$$0 = - u \frac{\partial T}{\partial x} - w \frac{\partial T}{\partial z} + D_V \frac{\partial^2 T}{\partial z^2} \tag{3}$$

and the continuity equation for two-dimensional steady flow:

$$0 = \frac{\partial u}{\partial x} + \frac{\partial w}{\partial z}, \quad \rho = \rho_o [1 - \alpha(T - T_o)] \tag{4}$$

---

*Numbers in brackets refer to references listed on page 31.

The terms are defined in the list of symbols and units. It is implied that Boussinesq's approximation can be used. Densities are treated as constants except in terms involving gravity, and temperature rises caused by internal friction are neglected. The density-temperature relationship in (x) is valid only over small temperature ranges.

Figure 2a displays the region to which the equations and the boundary conditions apply. The equation of convective heat transfer between the water surface and the air not shown in Fig. 2a is

$$h_s = k_s[T(x,0) - E] \tag{5}$$

This is an important additional boundary condition. E is the equilibrium temperature defined as the temperature of the water at which the net rate of heat exchange h_s will be zero.

The equations may be written in dimensionless form by using parameters at the warm water outlet as references:

U_o, average velocity at cooling water outlet for velocities

d_o, depth of cooling water outlet for lengths

ρ_o, density of warm water at outlet for density; this density used also as average density

T_o, temperature of warm water at outlet for temperatures

If the dimensionless quantities are designated by $\bar{u} = u/U_o$, $\bar{w} = w/U_o$, $\bar{T} = T/T_o$, and $\bar{p} = p/(\rho_o g d_o)$, the equations may be written as

$$0 = -\bar{u}\frac{\partial \bar{u}}{\partial \bar{x}} - \bar{w}\frac{\partial \bar{u}}{\partial \bar{z}} - \left(\frac{g d_o}{U_o^2}\right)\frac{\partial \bar{p}}{\partial \bar{x}} + \left(\frac{\nu_H}{U_o d_o}\right)\nabla^2 \bar{u} \tag{6}$$

$$0 = -\bar{u}\frac{\partial \bar{w}}{\partial \bar{x}} - \bar{w}\frac{\partial \bar{w}}{\partial \bar{z}} - \left(\frac{g d_o}{U_o^2}\right)\frac{\partial \bar{p}}{\partial \bar{z}} + \left(\frac{g\rho d_o}{\rho_o U_o^2}\right) + \left(\frac{\nu_V}{U_o d_o}\right)\nabla^2 \bar{w} \tag{7}$$

$$0 = -\bar{u}\frac{\partial \bar{T}}{\partial \bar{x}} - \bar{w}\frac{\partial \bar{T}}{\partial \bar{z}} + \left(\frac{D_V}{U_o d_o}\right)\frac{\partial^2 \bar{T}}{\partial \bar{z}^2} \tag{8}$$

$$0 = \frac{\partial \bar{u}}{\partial \bar{x}} + \frac{\partial \bar{w}}{\partial \bar{z}} \tag{9}$$

$$\bar{\rho} = 1 - \alpha(\bar{T} - 1) \tag{10}$$

In addition to the equations governing momentum, mass, and heat flow, the boundary conditions must also be reduced to dimensionless form as shown in Fig. 2b.

The surface heat transfer equation can be reduced by relating the heat flow to the mass flow using $\bar{h}_s = h_s/(U_o T_o \rho_o c_p)$ and $\bar{T} = T/T_o$.

$$\bar{h}_s = \left(\frac{k_s}{U_o \rho_o c_p}\right)\left[\bar{T}(\bar{x},0) - \left(\frac{E}{T_o}\right)\right] \tag{11}$$

If the set of equations could be solved for the given set of boundary conditions, the dimensionless results would obviously depend on the numerical value of the dimensionless groups in both the equations and the boundary conditions. Theoretically, mass-transfer, momentum-transfer, and heat-transfer similitude between models of different sizes or between model and prototype is achieved only if the dimensionless groups are numerically equal in models and prototype.

The flume experiments discussed in this report have no direct equivalent in nature, and the results obtained cannot be immediately applied to any real cooling water outlet. Nevertheless, it is felt that such experiments have a very important function because they provide an excellent means for understanding the complicated flow and exchange phenomena. Quantitative results can be used for validating prediction methods before their application to truly three-dimensional flow situations.

Results of flume experiments depend on the numerical values of the dimensionless groups. There are three categories of dimensionless groups describing the geometrical boundaries of the flume, the dynamics and kinematics of the flow, and the heat transfer processes, respectively.

One finds in the first category

$$\frac{d_\ell}{d_o}, \quad \frac{\ell_o}{d_o}, \quad \frac{\ell_t}{d_o}, \quad \frac{d_g}{d_o}, \quad \frac{\ell_\ell}{d_o}$$

in the second category

$$\frac{U_\ell}{U_o}, \quad \frac{gd_o}{U_o^2}, \quad \frac{\nu_H}{U_o d_o}, \quad \frac{g\rho d_o}{\rho_o U_o^2}, \quad \frac{\nu_V}{U_o d_o}$$

and in the third category

$$\frac{T_\ell}{T_o}, \quad \frac{E}{T_o}, \quad \frac{D_V}{U_o d_o}, \quad \frac{k_s}{U_o \rho_o c_p}$$

It appears that not all these groups are independent of each other. The eddy viscosities ν_H and ν_V depend on the turbulence characteristics of the flow. If the length scale, the velocity scale, and the viscosity of the fluid are considered sufficient to characterize the turbulence of the flow, the terms involving ν_H and ν_V can be replaced by a single dimensionless number, $\nu/U_o d_o$, because the velocity and length scales have already been expressed in other dimensionless parameters. A similar argument may be applied to the vertical eddy diffusivity D_V.

The fourth term in the second category and the last term in the third category can be written as

$$\left(\frac{g\rho d_o}{\rho_o U_o^2}\right) = \left(\frac{gd_o}{U_o^2}\right) + \left(\frac{g\Delta\rho d_o}{\rho_o U_o^2}\right)$$

and

$$\left(\frac{k_s}{U_o \rho_o c_p}\right) = \left(\frac{\nu}{U_o d_o}\right)\left(\frac{k}{\nu \rho_o c_p}\right)\left(\frac{k_s d_o}{k}\right)$$

respectively. The first term on the right-hand side of each expression has appeared previously.

The local values of the kinematic viscosity ν and of the density difference $\Delta\rho = \rho - \rho_o$ depend on the local fluid temperature. In dimensionless forms temperatures are taken with reference to the outlet temperature, and local ν and $\Delta\rho$ values may also be taken with reference to the outlet. Therefore, ν may be replaced by $\nu_o = \mu_o/\rho_o$ and $\Delta\rho$ by $\Delta\rho_o = \rho_\ell - \rho_o$. A reduced gravitational acceleration $g' = g\,\Delta\rho_o/\rho_o$ can also be defined.

The total set of dimensionless parameters may then be stated as

$$\frac{d_\ell}{d_o}, \quad \frac{\ell_o}{d_o}, \quad \frac{\ell_t}{d_o}, \quad \frac{d_g}{d_o}, \quad \frac{\ell_\ell}{d_o}$$

$$\frac{U_\ell}{U_o}, \quad \frac{gd_o}{U_o^2}, \quad \frac{\nu_o}{U_o d_o}, \quad \frac{g'd_o}{U_o^2}$$

$$\frac{T_\ell}{T_o}, \quad \frac{E}{T_o}, \quad \frac{k}{\mu_o c_p}, \quad \frac{k_s d_o}{k}$$

Five of these expressions are equal to or products of the following numbers:

Froude number $Fr_o = U_o(gd_o)^{-1/2}$

Reynolds number $Re_o = U_o d_o \nu_o^{-1}$

Densimetric or reduced Froude number $Fr_o' = U_o(g'd_o)^{-1/2}$

Prandtl number $Pr_o = \frac{\mu_o c_p}{k}$

Biot number $Bi_o = \frac{k_s d_o}{k}$

The final form of the set of dimensionless parameters is

$$\frac{d_\ell}{d_o}, \quad \frac{\ell_o}{d_o}, \quad \frac{\ell_t}{d_o}, \quad \frac{d_g}{d_o}, \quad \frac{\ell_\ell}{d_o}$$

$$\frac{U_\ell}{U_o}, \quad Fr_o, \quad Re_o, \quad Fr_o'$$

$$\frac{T_\ell}{T_o}, \quad \frac{E}{T_o}, \quad Pr_o, \quad Bi_o$$

For several reasons it was not necessary to investigate the effect of every dimensionless group separately.

Flow into essentially stagnant impoundments was to be investigated. Therefore the ratio U_ℓ/U_o was kept very small in all tests. It had to be different from zero, however, because cold water is entrained or heated by the discharged warm water. These effects have to be compensated for if a steady flow condition of warm water over a cold pool is to be obtained.

The real length of the outlet channel was without significance because a fully developed or nearly fully developed velocity profile was obtained in the outlet cross section in all tests. The channel bottom and flume walls were hydraulically smooth.

The height of the gate at the end of the flume was used to adjust the water depth in the outlet channel. The gate was a sharp-crested vertical weir, 5 in. wide, allowing the formation of a ventilated nappe. Total water depth in the flume, weir height, and total volumetric flow rate through the flume are related by the weir equation. Total flow rate and warm water flow rate are approximately proportional to the outlet Reynolds number because of the relationship $Q_o = U_o d_o = Re_o\, \nu_o$, where the kinematic viscosity ν_o does not vary over a wide range. Therefore the tailgate depth may be calculated from other dimensionless numbers with good approximation.

Sometimes a skimmer wall in the flume was used to control the interface independently from the total depth.

The squares of the Froude number Fr_o and the reduced Froude number Fr_o' are both ratios of inertial to gravitational forces. The derivation of the dimensionless numbers shows that the Froude number Fr_o has no bearing on the result if the gradient of the static pressure in the x-direction is zero and if the static pressure distribution in the z-direction is hydrostatic. Under these conditions the term

$$\left(\frac{g d_o}{U_o}\right) \frac{\partial \bar{p}}{\partial \bar{x}}$$

drops out of the equation of motion for the x-direction, and the pressure and gravity terms for the equation of motion in the z-direction become essentially

$$-\left(\frac{g d_o}{U_o}\right) \frac{\partial \bar{p}}{\partial \bar{z}} + \left(\frac{g \rho d_o}{\rho_o U_o^2}\right) = -\left(\frac{\rho_o - \rho}{\rho_o}\right)\left(\frac{g d_o}{U_o^2}\right) = \left(\frac{g' d_o}{U_o^2}\right)$$

The Froude number Fr_o thus disappears from both equations, and only the reduced Froude number is left.

It is believed that the above conditions are very nearly satisfied in the flume experiments and that the real Froude numbers Fr_o need not be recorded.*

The Prandtl number is the ratio of the kinematic viscosity of the fluid to its thermal diffusivity. Kinematic viscosity is often referred to as the molecular diffusivity of momentum. Thermal diffusivity is a measure of the ratio between the heat transmission and energy storage capacities of molecules. The molecular diffusivity of momentum changes with temperature. It is felt that in the flume experiments the temperature range is narrow enough $(60^{\circ}F < T_o < 90^{\circ}F)$ to justify the omission of the Prandtl number in the analysis.

In conclusion it appears that the dimensionless groups to be retained as variables in the flume experiments are

$$\frac{d_\ell}{d_o},\ \frac{\ell_t}{d_o},\ Re_o,\ Fr_o',\ \frac{T_\ell}{T_o},\ \frac{E}{T_o},\ Bi_o$$

---

*In a system of two horizontal layers of different densities the above conditions imply that the slope of the free water surface and the slope of the interface are related by an expression of the form

$$\frac{S_s}{S_i} = \frac{\Delta\rho}{\rho_o}$$

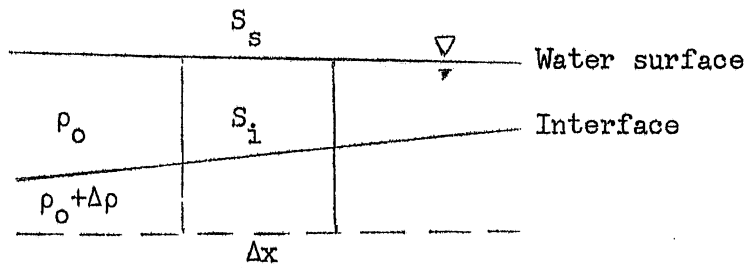

It is not necessary to make the assumption that the water surface is horizontal.

Processes involving surface heat transfer--that is, heat exchange through an interface--are usually described using the dimensionless Fourier modulus. For the purpose of the flume experiments involving heat loss through the water surface the Fourier modulus for the outlet may be written as

$$Fo_o = \frac{k_s}{\rho c_p} \frac{t_o}{d_o^2} \tag{12}$$

The expression $t_o = d_o/U_o$ can be used as reference time. The Fourier modulus is equivalent to the ratio of a Biot number to a Reynolds number and does not require a separate listing.

$$Fo_o = \frac{k_s}{\rho c_p \nu_o} \frac{\nu_o}{U_o d_o} = \frac{Bi_o}{Re_o}$$

A similar argument explains why the Nusselt number usually found in descriptions of convective heat transfer processes does not appear in the list of dimensionless groups. For the flume experiments the Nusselt number can be defined in various ways. It does not represent a "new" number, however.

$$Nu_o = f(Re_o, Pr_o) \tag{13}$$

It can be shown that the Nusselt number is a function of the Reynolds number, Re_o, and the Prandtl number, Pr_o.

In all experiments performed the width of the flume was $b = 0.5$ ft and the depth of the cold water layer $d_\ell = 0.75$ ft. The length of the flume used was $\ell_t = 25$ ft in most experiments. In a few cases this length was reduced down to a minimum of $\ell_t = 6$ ft. The main variable parameters were the outlet depth d_o (0.03 to 0.375 ft), the warm water flow rate Q_o (0.001 to 0.007 cfs), and the warm water temperature (60° to 90°F). The equilibrium temperature E could not be controlled. The flume was mounted in a portion of the building where only artificial light was used and temperature was controlled by a thermostat. Water left in the flume over a longer period of time (at least 24 hours) assumed equilibrium temperature E by definition. A survey of these temperatures showed that E was generally 4°F below the air temperature for average moisture conditions in the room. Room temperatures were recorded.

The cold water temperature could be controlled and varied roughly from 40°F to 65°F. As a result of these variations the dimensionless groups covered roughly the following range of main values:

$$\frac{d_\ell}{d_o} \quad 25 \text{ to } 2.0$$

$$\frac{\ell_t}{d_o} \quad 833 \text{ to } 66.7$$

$$Re_o \quad 100 \text{ to } 1800$$

$$Fr_o' \quad 0.2 \text{ to } 6.0$$

$$\frac{T_\ell}{T_o} \quad 0.6 \text{ to } 0.95$$

$$\frac{E}{T_o} \quad 0.8 \text{ to } 1.0$$

$$Bi_o \quad 0.18 \text{ to } 4.0$$

It is worth mentioning that the numerical values of these same parameters calculated for the Allen S. King Generating Plant on Lake St. Croix [4] as a prototype example fall into the same range of numbers, with two exceptions: the Reynolds number in the prototype is larger by a coefficient of 10^3 than in the flume experiments and the Biot number larger by a coefficient of about 10^2.

To show the effects of these differences the basic dimensionless equations (6), (7), (8), and (11) may be rewritten using the definitions of Reynolds, Biot, Prandtl, and Froude numbers as well as the assumption of hydrostatic pressure distribution.

$$0 = -\bar{u}\frac{\partial \bar{u}}{\partial \bar{x}} - \bar{w}\frac{\partial \bar{u}}{\partial \bar{z}} + \frac{\nu_H}{\nu_o}\frac{f_1}{Re_o}\nabla^2 \bar{u} \tag{6a}$$

$$0 = -\bar{u}\frac{\partial \bar{w}}{\partial \bar{x}} - \bar{w}\frac{\partial \bar{w}}{\partial \bar{z}} + \frac{f_2}{(Fr_o')^2} + \frac{\nu_V}{\nu_o}\frac{f_1}{Re_o}\nabla^2 \bar{w} \tag{7a}$$

where f_1 and f_2 are coefficients whose numerical values depend on local temperature T as well as on T_o and T_ℓ.

$$0 = -\bar{u}\frac{\partial \bar{T}}{\partial \bar{x}} - \bar{w}\frac{\partial \bar{T}}{\partial \bar{z}} + \frac{D_V}{\nu_o}\frac{1}{Re_o}\frac{\partial^2 \bar{T}}{\partial \bar{z}^2} \tag{8a}$$

$$\bar{h}_s = \frac{Bi_o}{Re_o}\frac{1}{Pr_o}\left[\bar{T}(\bar{x},0) - \left(\frac{E}{T_o}\right)\right] \tag{11a}$$

An examination of the first three of these dimensionless equations shows that any change in Reynolds number will affect the value of the last term in each of the equations. While this may not be of great significance for Eq. (6a), or for Eq. (7a), where the terms refer to fluid flow resistance, it will be of importance in Eq. (8a), dealing with temperature transport. This is because the relationship between the eddy viscosities ν_H and ν_V, the eddy conductivity D_V, and the Reynolds number Re_o is rather complex. Only if all these values were proportional to each other could scale effects be neglected. In conclusion, it may be stated that the failure to duplicate Reynolds and Biot numbers in a hydraulic model has two immediate consequences:

1) Phenomena associated with turbulence, such as convective mass and heat transfer processes, are not adequately represented in a three-dimensional hydraulic model; neither is momentum exchange. This bears on the frictional resistance which the warm water outflow experiences, on the formation of waves and vortices, and on the vertical temperature distribution.

2) The rate of heat loss at the water surface is much too high in a hydraulic model.

It is sometimes stated in the literature, though not entirely accurately, that the turbulent momentum and mass exchange do not seem to be substantially affected by the order of magnitude of the Reynolds numbers as long as the flow is in the turbulent range. There is also a question as to whether the Reynolds number alone is sufficient to adequately characterize turbulent flow.

The difference in the rapidity of the cooling process, however, is substantial. As a result the temperature decrease with distance from the outlet is not representative in a hydraulic model if precautions are not taken. Temperatures at large distances from the outlet are related to outflow conditions, but in substantially different ways in the experimental and natural environments.

4. Analysis of Results

4.1 Two-Layered, Inviscid Stratified Flow near a Surface Outlet

4.11 Shape of the Interface and Location of Controls -- A simplified model assuming two-layered, inviscid stratified flow is useful in defining the extent to which the flow conditions at the outlet itself control the cooling water flow pattern. The only heat exchange processes considered are those tied to mass transfer; viscous shear forces are neglected. It is assumed that the density gradient between the warm and cold layers is strong and that no convective exchange between the two layers takes place. The layers are homogeneous in themselves. The results of the analysis must be expected to reflect only qualitative aspects of the outlet flow.

According to the above assumptions (which may be quantitatively expressed by $k_s = 0$, $k = 0$, and $\nu = 0$) the dimensionless groups with significance for the problem are the geometrical ratios d_ℓ/d_o and ℓ_t/d_o and the reduced Froude number Fr_o'. It can thus be seen that the problem is analogous to that of classical open-channel flow. The interface between warm water and cold water is equivalent to the air-water interface. The gravitational acceleration g is replaced by an upward-directed, reduced acceleration g'.

The position of the interface between the non-viscous warm and cold water layers will be controlled by conditions found either at the warm water outlet into the flume or at the end of the flume. The behavior of elementary waves of very small amplitude on the interface may be used to indicate which end of the flume exerts control. If a disturbance consisting of an elementary interfacial wave is able to travel against the flow direction of the warm water layer, the flow is controlled by the tailgate and may be called "internally subcritical." If the elementary wave is carried downstream by the warm water flow the flow is controlled by the outlet, or is "internally supercritical." The velocity of an elementary interfacial wave with respect to the stagnant stratum is

$$v_w = \frac{U_1}{2} \pm \sqrt{c^2 - \left(\frac{U_1}{2}\right)^2} \qquad (14)$$

where U_1 is the velocity of the upper layer considered in uniform motion and c is the wave velocity which would be observed if both layers, of thicknesses d_1 and d_2, having a density difference $\Delta\rho$, were at rest.

$$c = \sqrt{g \frac{\Delta\rho}{\rho} \frac{d_1 d_2}{d_1 + d_2}} = \sqrt{g' \frac{d_1 d_2}{d_1 + d_2}} \tag{15}$$

These equations are quoted from Ref. [6]. In considering an elementary wave which travels against the flow of the upper layer the minus sign must be used. Flow will be outlet-controlled if $v_w > 0$ and tailgate-controlled if $v_w < 0$. The limiting or "critical" condition is found when $v_w = 0$ or

$$\left(\frac{c}{U_1}\right)^2 = \frac{1}{2} \tag{16}$$

The velocities and depths of the warm water layer, designated as U_1 and d_1, and the corresponding quantities for the outlet, designated as U_o and d_o, are related by

$$U_1 d_1 = U_o d_o \tag{17}$$

The condition therefore becomes

$$\frac{g' d_o}{U_o^2} \left(\frac{d_1}{d_o}\right)^3 \left(\frac{d_2}{d_1 + d_2}\right) = \frac{1}{2} \tag{18}$$

Since in a very deep reservoir $d_2 \gg d_1$, the above condition is close to

$$\left(\frac{d_1}{d_o}\right)^3 = \frac{(Fr_o')^2}{2} \tag{19}$$

This is the equation for a critical depth $d_{1Cr} = d_1$. If the depth of the warm water layer d_1 is less than the outlet depth, stratification may reach into the outlet channel and cold water penetrate into it, forming a cold water wedge. This situation is shown in Fig. 3.

The critical condition for interfacial wave propagation into the outlet channel is obtained if the substitution $d_2 = d_o - d_1$ is made in the previous equation. Thus the relationship

$$\left(\frac{d_1}{d_o}\right)^3 \left(1 - \frac{d_1}{d_o}\right) = \frac{(Fr_o')^2}{2} \qquad d_1 < d_o \tag{20}$$

is obtained. The two critical relationships, one for the deep reservoir and one for the outlet channel, have been plotted in Fig. 4.

Also shown in Fig. 4 are lines which result from application of the principles of conservation of energy and impulse momentum. For a warm water discharge at a given reduced Froude number Fr_o' the warm water layer d_1 having the same total energy can be found from the relationship

$$\frac{\rho U_o^2}{2} - \frac{\rho U_1^2}{2} = (d_1 - d_o) g \Delta\rho - S_w \Delta x g \rho$$

where S_w is the slope of the water surface. If the second term on the right-hand side of the equation is much smaller than the first term (as is the case when shear is neglected), the equation may be reduced to

$$\frac{Fr_o'^2}{2} = \frac{\frac{d_1}{d_o} - 1}{1 - \left(\frac{d_o}{d_1}\right)^2} \tag{21}$$

The continuity equation was also used to obtain this result.

Application of the impulse-momentum theorem produces a relationship for the conjugate depths in an internal hydraulic jump as shown in Ref. [7]. The flow from the warm water outlet may produce an internal hydraulic jump, but the outlet depth d_o is rarely one of the conjugate depths, because the free interface is missing. Nevertheless, the relationship has been plotted for the purpose of comparison.

4.12 Interfacial Waves -- At the interface between two layers of fluids of different densities, periodic gravity waves may form. Stable as well as unstable waves may be found. The velocities of periodic interfacial waves have been given in Eqs. (26.24) and (26.25) in Ref. [8]. Applying these equations to a two-layered system in which the upper layer is flowing at uniform velocity U_1 and the lower layer is at rest, it can be shown that a

real wave velocity will be obtained only if

$$\frac{1 + \coth (2\pi d_1/L)}{\coth (2\pi d_1/L)} > 2\pi \frac{U_1^2}{g'L} \qquad (22)$$

Experimental data gathered during this study suggest that the waves break when the ratio d_1/L--that is, the ratio of the depth of the surface layer to the wave length--takes a numerical value between π and 2π. This may be compared with the value of $d_2/L = \pi$ found by several authors for bottom density currents [6], [8]. The shape of waves forming in a channel depends apparently on the reduced Froude number at the outlet. Wave lengths decrease as the waves change from non-breaking waves to breaking waves. This phenomenon was also observed in a series of unpublished experiments dealing with bottom currents rather than surface currents.

If the ratio d_1/L for breaking waves were equal to π, with d_1 the thickness of the upper layer, the condition for wave breaking would become $Fr_1' = 1.33$. If the ratio d_1/L were equal to 2π, then Fr_1' would equal 1.40. Since these are not very different values, the lack of precise information on the critical (d_1/L) value is not a serious problem. The critical Froude number Fr_1' may be considered to be close to 1.35, indicating that waves should be breaking for any value larger than this.

Since the Froude number of the upper layer, Fr_1', and the outlet Froude number, Fr_o', are related by

$$\frac{Fr_1'}{Fr_o'} = \left(\frac{d_o}{d_1}\right)^{3/2}$$

the critical condition for interfacial stability is

$$Fr_o' = 1.35 \left(\frac{d_1}{d_o}\right)^{3/2} \qquad d_1 > d_o \qquad (23)$$

This relation is also shown in Fig. 4.

4.2 Two-Layered, Viscous Stratified Flow near a Surface Outlet

Application of the impulse-momentum principle and other equations to the outlet flow is likely to produce somewhat unrealistic results if viscous effects are ignored. Forces caused by shear stresses are likely to be of the same order of magnitude as forces due to normal stress in the range of the interface discontinuity. It is necessary to introduce viscous effects into Fig. 4 to obtain more than a qualitative picture.

4.21 Shape of the Interface -- Starting from the equations of motion for stratified flow given in Ref. [9] it can be shown that the differential equation describing the interface of a two-layered system with the lower layer at rest is

$$\frac{dy}{dx} = \frac{\rho}{\Delta\rho} \frac{S_2 - S_1}{1 - (Fr_1')^2} \tag{24}$$

with $$S_2 = \frac{\tau_b + \tau_i}{\rho d_2 g}, \quad S_1 = \frac{-\tau_i}{\rho d_1 g}, \quad Fr_1' = \frac{U_1}{\sqrt{g' d_1}}$$

S_1 and S_2 are the slopes of the energy grade lines of the upper and lower layers and τ_i and τ_b are the shears at the interface and the channel bottom, respectively.

The differential equation is a more general form of the steady, gradually varied flow equation for open channels. It can be solved if an expression for the shear is introduced into the differential equations. Numerical solutions using finite differences will normally prove adequate.

If the control is at the tailgate, which is generally the case, calculations can start with the internal critical depth

$$d_{1c} = \sqrt[3]{\frac{q_1^2}{g'}}$$

at the end of the flume and proceed upstream as sketched in Fig. 5. Any one of the interface profiles near the warm water outlet shown in Fig. 6 can be obtained in this way if the flow is tailgate-controlled in the whole flume.

If there is enough shear, periodic waves may be superimposed on the interfacial profiles. These are called Type B flow in contrast to the original or Type A flow shown in Fig. 6.

If control of the flow takes place at the outlet, calculations of the interface must proceed in the flow direction starting at the outlet much as in water profile computations in supercritical open-channel flow. Since outlet-controlled flows are generally associated with instability of the interface and, more commonly, strong turbulence, such computations are of little value, since the results which they produce do not conform to reality.

4.22 Interfacial Waves and Effects of Turbulence on the Interface -- A horizontal layer of warm water flowing over another horizontal layer of essentially stagnant cold water exerts shear on the latter. This causes a flow in the colder water. In addition, waves may also be generated in a manner simulating wave generation by wind blowing over water. The Miles-Benjamin theory states the circumstances under which this phenomenon occurs, but this theory is not applicable to warm water flow because it contains the assumption that the upper layer is not disturbed by the wave phenomenon. This may be permissible in the case of air, but it is not for water.

The onset of interfacial waves must therefore be defined on an experimental basis. Since the waves are moving because of gravity forces and generated by shear forces, a function

$$f(Fr_o', Re_o) = 0$$

must define the limiting conditions under which waves are generated and stable. Dimensional considerations show that an expression such as

$$Re_o(Fr_o')^n < C \qquad (25)$$

must be satisfied if stability of the interface is required. According to Keulegan [6] the following constants may be considered indicative:

n	C	Type of Flow
3/2	440	One stratum much thinner than the other
3/2	77,000	Strata of same large thickness

Interfacial waves generated by shear, whether breaking or not, are characterized by regularity in contrast to other interfacial disturbances caused by, for example, turbulence or eddies.

It was noted in the experiments that if waves form, they usually appear at a short distance (0.5 to 1.0 ft) from the outlet, increase in amplitude, and decay into irregular interface disturbances about 3 to 4 ft from the outlet. The train of waves usually consists of no more than 2 to 5 clearly defined waves. Usually a second train of waves with smaller amplitudes forms downstream about 6 ft in the flume. From about 10 ft on the interface usually is very flat and undisturbed. These observations and the fact that in none of the experiments did a regular wave pattern appear over a larger portion of the flume seem to justify the preliminary conclusion that the feedback of the waves to the upper layer must have an effect such as to prevent uniform formation of waves by shear flow.

It is obvious that at the point of discharge of warm water only the upper layer is continuous, whereas the lower layer is limited by a vertical or inclined wall. This is important when stability theories are applied to the problem. Theoretical assumptions and experimental conditions are not identical.

To define the critical conditions for the formation of waves of different kinds, tests were run in which the bottom of the outlet channel was tangent to the interface. This could be controlled from the tailwater if the flow was subcritical. An additional gate in the channel was used to allow the elevation of the water surface and that of the interface to be controlled independently. The experimental data collected are presented in Fig. 7 along with the exponential function $Re_o (Fr_o')^{3/2} = 440$ which is supposed to separate stable and unstable stratified flow regions. The results presented in Fig. 7 show good agreement of experimental values in subcritical flow with the equation proposed in Ref. [6]. The range of values covered is, however, quite small. The equation also seems to describe the limit of beginning wave formation in the laminar two-dimensional jet quite well. The onset of wave instability at very low Reynolds numbers and reduced Froude numbers satisfies an equation of the proposed type, but with an exponent n closer to 1/2 than to 3/2. A possible reason for this is that for supercritical flow at the outlet the flow downstream is not uniform, but increases in thickness.

A certain length or distance from the outlet is required so that the waves, breaking or not, can form. Even if the angle of expansion of the laminar jet is small in homogeneous fluid flow and is further reduced by buoyancy forces in two-layered flow, the depth of the warm water layer at the point of observation, which is generally from 0.5 to 4 ft downstream, is greater than at the outlet. The outlet Froude number is therefore probably too large to be used as a reference value.

Also shown in Fig. 7 are lines $Re_o = 500$ and $Fr_o' = 1$, which serve as guidelines to limit very roughly the areas of laminar and turbulent flow as well as of subcritical and supercritical flow.

A discussion of interfacial stability near the outlet must also consider the effects of turbulence and eddies shed from the outlet on the interface. These are of great importance when the outlet flow is subcritical and the tailgate-controlled interface has a shape such as that of curves A-2 and B-1 in Fig. 6.

Observation of the time-dependent behavior of the interface was accomplished with dye entrained from potassium-permanganate crystals deposited on the bottom of the outlet channel. The "visual interface" was determined to be at the elevation of the smallest amount of vertical dye dispersion or mixing. The interface may be very smooth in appearance or slightly roughened like the surface of a liquid exposed to wind. The irregular disturbances may eventually separate from the interface, leading to a small amount of mixing. The rough appearance of the interface is caused by the turbulence of the flow. The natural turbulence may be augmented by decaying vortices. In some instances the vortices found at the outlet may reach the interface and augment mixing. It must be expected that the interfacial stability in such cases depends also on the Re_o and Fr_o' numbers at the outlet and the depth ratio d_1/d_o.

4.3 Interference of Outlet Flow with Tailgate-Controlled Interfaces

Numerous experiments were carried out to study the flow of warm water from the outlet into the flume. Among the variables tested it was apparent that the magnitude of the reduced Froude number at the outlet, Fr_o', influenced the flow more than any of the other parameters.

At low numerical values of the reduced Froude number at the outlet the warm water discharge does not affect the shape of the interface or the interfacial stability or mixing process. The cold water may even penetrate into the outlet channel. Fig. 6 shows schematically some examples of the interface positions. The depth of the interface below the water surface depends on the position of the tailgate, the discharge, and the temperature difference. The flow is internally subcritical in the sense that any modification of the depth of flow downstream will be propagated upstream.

As the reduced outlet Froude number is increased, the interface will become increasingly rough, and eventually a mixing wedge will form. This mixing wedge has a roughly triangular shape and rides as a kind of intermediate layer on top of the interface. The mixing wedge consists essentially of fluid mixed at the interface and circulating back to the outlet, where it is entrained by the warm water jet. This type of flow is labeled "Type C" and is shown in Fig. 8.

The Type D flow sketched in Fig. 8 was obtained at higher reduced Froude numbers than Type C. It is a two-dimensional jet with some backflow caused by buoyancy. It looks very much like an inverted hydraulic jump, but the term should be avoided because outlet and downstream depth are not necessarily conjugate depths as defined in open-channel flow.

The last possible stage is that of a regular two-dimensional jet. Buoyancy effects are entirely overcome by inertial and viscous effects caused by high outlet velocities (Type E flow). Types C, D, and E, shown in Fig. 8, are associated with a substantial amount of mixing.

It can be seen that the actual depth downstream from the outlet depends entirely on the tailgate conditions. The type of "outlet-controlled flow" will therefore depend not only on the outlet Froude numbers, but also to a very great extent on the downstream conditions, though they may not be intended to affect the outfall flow problem. This is true no matter what the end of the flume looks like. Therefore, different types of flow may be developed for one outlet flow condition that has a constant reduced Froude number Fr_o' and Reynolds number Re_o' at the outlet.

The tailgate in the flume has no equivalent in nature. Instead, the cooling process will play the role of the tailgate. Thus the problem is extremely complex.

At this point it may be useful to present measurements of temperature profiles in the flume for various outlet conditions in support of the discussion. The following types of flow were observed:

Type	Fr_o'	Re_o
A-1	0.29	450
A-2	0.33	930
D	2.0	1320
D	6.5	1420

Results are shown in Figs. 9a through 9d.

The various types of flow obtained are also shown in Figs. 10a and 10b for low and high Reynolds numbers, respectively. The separation was made because in laminar flow the flow patterns obtained in the flume are substantially different from those sketched in previous figures relating to turbulent flow, which is of sole interest in prototypes.

4.4 Heat and Mass Transfer Between Flowing and Essentially Horizontal Layers of Different Temperatures

Before dealing with the very complicated mixing process near the outlet which may occur if the reduced outlet Froude numbers are high enough, some attention will be given to the transport process associated with an essentially horizontal flow of warm water on top of cold water.

Measurements of temperatures and velocities in the flume have shown that it is possible to distinguish between flow with established and essentially horizontal stratification and particular exchange phenomena. Horizontal stratified flow is usually found at greater distances from the outlet, while particularly strong exchange phenomena may occur only near the outlet itself.

It is usually possible to identify both an outlet mixing region and a stratified flow region away from the outlet. The initial temperature and velocity profiles of the stratified flow region usually show the following distinct zones: An upper zone in which both temperature and velocity are rather uniform, a buffer zone with a very strong temperature gradient which

suppresses turbulent transport in the vertical direction, and a lower zone with again fairly uniform temperature and velocity. While the stratification does not inhibit momentum transport by shear, a strong initial temperature gradient which is accompanied by a density gradient substantially reduces the mean free path of the eddies in turbulent flow. Vertical turbulent mass and convective heat exchange are thus greatly reduced. Disturbances in the flow are damped out more rapidly and the stability of the flow is greatly increased. A measure of this local stability is the Richardson number, defined as

$$Ri = \frac{-g \frac{d\rho}{dz}}{\rho \left(\frac{du}{dz}\right)^2} \tag{26}$$

Figs. 11a and 11b show velocity and temperature distributions measured in two early experiments. The Richardson number distributions were obtained numerically. Because of considerable scatter in the calculated Richardson numbers it was decided to fit the experimental velocity and temperature data to the analytical expressions shown below and to use these to find Richardson numbers.

Figure 11c shows temperature and velocity distributions which have developed at 6 ft from the outlet, where the discharge was made with Re_o equal to 196, Fr_o' equal to 4.1, and an initial depth of 0.017 ft. Over the first two feet past the outlet a two-dimensional laminar jet and breaking waves formed. Then the flow became nearly horizontally stratified. The temperature data can be converted into density data. A function which fits the density data fairly well is

$$\rho = \rho_{max} - \Delta\rho \exp\left\{-\frac{(z - z_T)^2}{2\sigma^2}\right\} \tag{27}$$

where $\rho_{max} = \rho_\ell$ is the density of the cold water, $\Delta\rho$ is the maximum density difference between warm and cold water, z_T is the depth of the point of maximum temperature below the water surface, and σ is the standard deviation or distance from the temperature maximum to the temperature

inflection point. Similarly the velocity data fit fairly well a curve described by the equation

$$u = u_{min} - \Delta u \exp\left\{\frac{-z}{n}\right\} \tag{28}$$

The Richardson number distribution which results from these two equations is also plotted in Fig. 11. The characteristic features of this curve are the low Ri value near the water surface, the large increase in Ri values with depth across the interface, and the peaking and subsequent decrease in Ri values at greater depths.

Ellison and Turner [10], as well as other investigators, have shown how local mass exchange depends on local Richardson numbers. According to their findings entrainment by turbulence is greatly reduced when the Richardson number is more than the critical Richardson number which has a value between 0.1 and 1.0. This is in agreement with the observations recorded in Fig. 11.

The visual interface indicated in Fig. 11 is a zone in which dye which is released at the warm water channel bottom accumulates or remains in larger concentration than elsewhere. This zone is usually very thin and is caused by the absence of turbulent mixing and entrainment. At the depth of the visual interface the Richardson number must be critical or larger than critical. The smallest Richardson number associated with the interface in about 20 experiments was found to be 3.5. It may therefore be concluded that the critical Richardson number must be less than or equal to this value.

In a stably stratified horizontal flow the development of temperature profiles should indicate where temperature is transported essentially by convection and where it is transported by conduction only. For this evaluation the heat transport equations may be used. In an essentially horizontal flow with a temperature gradient the equation of heat transport is

$$0 = - u \frac{\partial T}{\partial x} + \frac{\partial}{\partial z}\left(D_V \frac{\partial T}{\partial z}\right)$$

where the vertical eddy diffusivity D_V is a function of depth. The coefficient of turbulent heat exchange can be found from the relationship

$$D_V = \left(\frac{\partial T}{\partial z}\right)^{-1} \int_{-\infty}^{z} u \frac{\partial T}{\partial z} \, dz \tag{29}$$

if the velocity profile is fully developed and the flow steady, incompressible, and horizontal. Measurements of the temperature profiles 6 and 12 ft from the outlet, respectively, and the velocity profile were used to evaluate the turbulent coefficient of vertical convective heat exchange. The temperature gradients in the x direction are usually small and therefore hard to evaluate. Nevertheless, the results obtained seem of enough interest to be shown in Fig. 12. It is felt that the absolute values of the dimensionless heat exchange coefficient may not be reliable, but that the general trend is correct. The figure also indicates that convection disappears at Richardson numbers between one and ten. The decrease in values of Richardson number with distance may be explained by the effect of conduction.

To obtain more information on the transport process, temperatures were converted to densities and the ratio $(\rho - \rho_c)/(\rho_w - \rho_c)$ plotted versus depth on probability paper. The reasoning behind this procedure is that in many of the flume experiments heat transport by convection was observed in the uppermost part of the warm water layer. The flow was turbulent and the temperature gradients were small. At greater depths the temperature gradient is stronger and the Richardson numbers are high enough to prevent any convective transport. Heat transport is reduced to conduction alone. Underneath this zone, which may be called a "buffer zone," convective mixing takes place again. In the buffer zone the equation of heat transport is

$$0 = - u \frac{\partial T}{\partial x} + \frac{k}{ac} \frac{\partial^2 T}{\partial z^2} \tag{30}$$

If the buffer zone is thin enough to justify the assumption that u is constant, the substitution of $t = x/u$ will reduce the heat flow equation to the diffusion equation

$$0 = - \frac{\partial T}{\partial t} + \frac{k}{ac} \frac{\partial^2 T}{\partial z^2} \tag{31}$$

where $k/\rho c_p = a$ is the thermal diffusivity.

The temperature profile in the buffer zone may therefore be considered the result of a diffusion process starting with a temperature jump $T_w - T_c$ at the temperature inflection point at time $t = 0$. The temperature profile then develops according to the equation

$$\frac{T - T_c}{T_w - T_c} = \frac{1}{2} \pm \frac{1}{2} \operatorname{erf} \left(\frac{z_i - z}{2\sqrt{at}} \right) \tag{32}$$

where T is the temperature at time t and depth z below the water surface, z_i is the depth of the temperature inflection point, and T_w and T_c are the temperatures of the warm and cold water, respectively, at time $t = 0$. The relationship will plot as a straight line on probability paper. Density differences may be used instead of temperature differences in the above equation if the temperature range is not too wide, since a linear relationship between density and temperature can be used for temperature differences of only a few degrees Fahrenheit.

In the flume experiments flow is nearly horizontal at several feet from the outlet. In a deep reservoir and with a fully developed velocity profile, flow velocities are nearly uniform in the upper part of the impoundment. The limited depth of the warm layer should not present a serious limitation to the application of the diffusion equation to the buffer zone.

Figure 13a shows density differences plotted on probability paper against depth for one test. The densities were derived from temperatures. Near the inflection point results plot nearly as a straight line, indicating that there is a buffer zone with the aforementioned properties.

There is a layer of fluid on either side of the inflection point of the temperature profile in which the heat exchange coefficient, or thermal diffusivity, is nearly constant. The thickness of that layer apparently decreases with distance from the outlet, indicating that the buffer zone becomes thinner.

The slope of the temperature profile at the inflection point and the thermal diffusivity are related by the equation

$$a = \frac{(T_w - T_c)^2}{(\partial T/\partial z)^2} \quad \frac{1}{4\pi t} \quad \text{at} \quad z = z_i \tag{33}$$

or, in finite difference form for densities,

$$a = (\rho_w - \rho_c)^2 \left(\frac{\Delta z}{\Delta \rho}\right)^2 \frac{1}{4\pi t}$$

Because of some initial mixing at the outlet, time t is actually unknown. It is therefore desirable to eliminate the time by using measurements in two cross sections instead of one. If these are Δx feet apart, the time interval associated with them is approximately

$$\Delta t = \frac{\Delta x}{u} = \frac{\Delta x \, z_i}{q}$$

and the thermal diffusivity is

$$a = \frac{(\rho_w - \rho_c)^2}{4\pi \Delta t} \left[\left(\frac{\Delta z}{\Delta \rho}\right)_2^2 - \left(\frac{\Delta z}{\Delta \rho}\right)_1^2\right] \tag{34}$$

If the data in Fig. 13a are evaluated by this method, the following experimental values of the thermal diffusivity are found:

x (ft)	a_{exp} (ft^2/sec)	$\frac{a_{exp}}{a_{theor}}$
5 - 10	0	0
10 - 15	2.93×10^{-6}	1.79
15 - 20	2.66×10^{-6}	1.62

It can therefore be concluded that in the observed buffer zone heat transfer takes place almost by conduction alone. The effect of the buffer zone weakens with distance, however.

A plot of temperatures on probability paper for the test whose results are shown in Fig. 12 showed a buffer zone extending from 0.03 to 0.095 ft below the water surface between distances $x = 6$ ft and $x = 12$ ft from the outlet. The slope of the temperature profile yielded a value very close to unity in this zone, as was expected. The result is shown in Fig. 12.

The shape of the dimensionless density distribution in Fig. 13a indicates that outside the buffer zone the turbulent exchange coefficient is not uniform, a result obviously caused by stratification.

An interesting effect of strong interfacial stability after initially strong mixing is shown in Fig. 13b. The discharge takes place at $Re_o = 206$ and $Fr_o' = 4.6$. There is some initial mixing due to waves near the outlet, but between $x = 5$ ft and $x = 15$ ft from the outlet there is no additional mixing at all and very little conductive heat transport because the temperature gradient is small. Thus the temperature and density profile slopes remain practically constant over a substantial length. It may also be remarked that Fig. 13b refers to a stratification without a buffer zone. The dimensionless density distribution has almost no straight portion.

A simultaneous study of the dispersion of dye and temperature discharged by a jet into cold water should produce similar exchange coefficients if mixing is convective. Figure 14 shows the evaluation of a temperature and a dye concentration profile between $x = 6$ ft and $x = 12$ ft from the outlet in a very stable stratification. $Re_o = 227$ and $Fr_o' = 0.76$. There is no dye flow across the interface, and the dye concentration gradient at the interface increases with distance because of mixing in the upper and lower layers themselves. Despite an obvious lack of convection across the interface, heat is still transported by conduction and the temperature profile shows some heat flow across the interface.

Figures 12 and 14 refer to the same test. It can be seen that the Richardson numbers are quite high in the range of depths where convection has obviously disappeared due to stratification.

An evaluation of the dimensionless transport coefficient for heat and dye in the vicinity of the interface between $x = 6$ ft and $x = 12$ ft shows that for this particular test both dye concentration and temperature follow a normal probability distribution over a range of depths; the turbulent coefficient of mass exchange is zero in that range; and a deviation of concentration and temperature from the normal probability distribution is found at a depth at which the Richardson number is very close to unity.

In summary it may be said that the intensity of the heat exchange process in an essentially horizontal flow is highly variable according to the stability of the flow. The Richardson number seens to correlate well with the vertical turbulent transport. Sizable convective heat transport seems to take place only if the Richardson number is less than the critical value, the order of magnitude of which is near unity.

4.5 Heat and Mass Transport in the Vicinity of the Outlet

Only in particular cases was the flow in the immediate vicinity of the outlet found to be horizontal. Generally the thickness of the warm water layer near the outlet was much greater than the outlet depth because of the tailgate effect. Therefore the separation of streamlines at the terminal point of the outlet channel, the formation of eddies, and the eventual mixing could be observed quite often. The results of outlet mixing depend essentially on convection. Thus along with the outlet geometry Fr_o', Re_o, and d_ℓ/d_o are of primary importance in the process. While it is difficult to test the effect of Re_o in the laboratory, the two other parameters can be adjusted to values also found in three-dimensional prototype outlets. Results of such an investigation are shown in Fig. 15.

Temperatures were measured in the centerline of the test flume, i.e., 3 inches from the vertical walls. Variations over the width of the flume were found to be small. The largest deviations from the centerline temperature occurred in a very thin layer adjacent to the walls. Temperatures are reported as functions of depth below the water surface and for various distances from the outlet.

Areas in which temperatures were time-dependent are also shown. These temperature fluctuations were caused by either turbulent mixing of water of different temperatures or interfacial waves. The first situation arose near the outlet, the second further downstream.

After the initial outlet mixing--if any occurred--a strong stratification usually formed in all experiments. The visual interface generated by dye crystals at the bottom of the outlet channel could be clearly seen over the total length of the flume, indicating that there was a zone with practically no convective transport. Thus conduction was the only mechanism for heat transport from the upper layer to the lower layer, which were separated by the visual interface. The resulting temperature changes with distance were generally quite small. The great importance of the outlet mixing thus became strikingly evident.

5. Conclusions

The experimental data discussed in this report show that the flow from a warm water outlet into a colder reservoir cannot be described in terms of the geometry and flow conditions at the outlet alone. The effects of the flow through and out of the reservoir (tailgate) have been shown to be very strong. In an "unbounded" reservoir the role of the tailgate control is played by the surface cooling process. Thus the meteorological conditions (air temperature, humidity, wind velocity) are likely to affect the outlet flow strongly and make it necessarily an unsteady flow process because of diurnal and seasonal weather changes.

For engineering purposes the discharge conditions can be described adequately by the outlet geometry and the Reynolds number and densimetric Froude number at the outlet. A more precise description of the flow must also include temperature ratios of warm and cold water, the Prandtl number, and the ratio of air and water temperatures at the outlet. But these are not sufficient yet to predict which type of flow will occur.

Different types of flow near an outlet have been observed and defined. A relationship between reduced Froude number at the outlet, depth of the warm water layer in the receiving reservoir (relative to outlet depth), and type of flow has been shown qualitatively. The effect of outlet Reynolds number on the previous relationship was not studied. Only for interfacial stability could turbulence effects be shown experimentally.

The turbulent mixing process which may occur near the outlet is very different from that found at greater distances from the outlet. When stratification existed, turbulent exchange was observed to vanish at locations where the Richardson number was larger than 3.5. The critical Richardson number was found to be close to unity in a more detailed analysis of one experiment.

Conductive heat transfer cannot be ignored in laboratory experiments, whereas perhaps it can be in full-scale reservoirs. However, heat loss at the water surface and turbulence are relatively much larger in laboratory experiments than in full-scale situations. This is important in the interpretation of experimental results.

A sound motion picture entitled "Warm Water Flow into Impoundments" was prepared in the course of this study. The film shows some of the flow patterns from a warm water outlet into a cooler reservoir.

6. Acknowledgments

This study was carried out under the general supervision of Professor Edward Silberman, Director, St. Anthony Falls Hydraulic Laboratory. Mr. J. Pommerenke, Mr. N. Hayakawa, and Mr. E. Cloud took some of the data reported and carried out many of the numerical computations. Mr. Y. C. Shen assisted in the taking of preliminary data.

REFERENCES

[1] Stefan, H. and Schiebe, F. R., "The Measurement of Low Fluid Velocities with the Aid of a Tethered Sphere," Water Resources Research, Vol. 4, No. 6, December 1968.

[2] Schiebe, F. R.; Stefan, H.; and Hayakawa, N., Experimental Study of Warm Water Flow into Impoundments, Part II: Temperature and Velocity Instrumentation and Data Processing for the Three-Dimensional Flow Experiments, Project Report No. 102, St. Anthony Falls Hydraulic Laboratory, December 1968.

[3] Edinger, J. E.; Duttweiler, D. W.; and Geyer, T. C., "The Response of Water Temperatures to Meteorological Conditions," Water Resources Research, Vol. 4, No. 5, October 1968.

[4] Silberman, E. and Stefan, H., Effects of Condenser Cooling Water Discharge from Projected Allen S. King Generating Plant on Water Temperatures in Lake St. Croix, Project Report No. 76, St. Anthony Falls Hydraulic Laboratory, December 1964.

[5] Kreith, F., Principles of Heat Transfer, International Textbook Co., 3rd Printing, August 1960.

[6] Engineering Hydraulics, edited by H. Rouse: Chapter XI, Section 9, by G. H. Keulegan; Wiley and Sons, 1949.

[7] Yih, Chia-Shun and Guha, C. R., "Hydraulic Jump in a Fluid System of Two Layers," Tellus VII, 3, 1955, pp. 358-366.

[8] Handbook of Fluid Dynamics, edited by V. L. Streeter: Chapter 26, by D. F. Harleman; McGraw-Hill, 1961.

[9] Schijf, J. B. and Schönfeld, J. C., "Theoretical Considerations on the Motion of Salt and Fresh Water," Minnesota International Hydraulics Convention, September 1953.

[10] Ellison, T. H. and Turner, T. S., "Turbulent Entrainment in Stratified Flows," Journal of Fluid Mechanics, Vol. 6, 1959.

[11] Schlichting, H., Boundary Layer Theory (English translation), McGraw-Hill, 6th Ed., 1968.

LIST OF SYMBOLS AND UNITS

a = Thermal diffusivity ($ft^2\ sec^{-1}$)

b = Width of flume (ft)

c_p = Specific heat (BTU $slug^{-1}\ {}^oF^{-1}$)

d = Depth (ft)

D_V = Vertical eddy diffusivity ($ft^2\ sec^{-1}$)

E = Equilibrium water temperature for given atmospheric conditions (air temperature, humidity, wind velocity) (^oF)

g = Acceleration of gravity ($ft\ sec^{-2}$)

H = Heat flow rate ($BTU\ hr^{-1}$)

h_s = Rate of surface heat transfer per unit area by convection ($BTU\ hr^{-1}\ ft^{-2}$)

k = Thermal conductivity ($BTU\ hr^{-1}\ ft^{-1}\ {}^oF^{-1}$)

k_s = Average surface coefficient of heat transfer ($BTU\ hr^{-1}\ ft^{-2}\ {}^oF^{-1}$)

L = Wave length (ft)

ℓ = Length (ft)

p = Static pressure of fluid ($lbs\ ft^{-2}$)

Q = Volumetric flow rate in x direction ($ft^3\ sec^{-1}$)

S = Slope (-)

T = Temperature (^oF)

t = Time (sec)

u = Fluid velocity in x direction ($ft\ sec^{-1}$)

v = Fluid velocity in z direction ($ft\ sec^{-1}$)

x = Horizontal coordinate (ft)

z = Vertical coordinate (ft)

SYMBOLS AND UNITS (Continued)

α = Coefficient of volume expansion ($^{o}F^{-1}$)

ν = Kinematic fluid viscosity ($ft^2\ sec^{-1}$)

ν_H = Horizontal eddy viscosity ($ft^2\ sec^{-1}$)

ν_V = Vertical eddy viscosity ($ft^2\ sec^{-1}$)

ρ = Density of fluid ($slugs\ ft^{-3}$)

$\Delta\rho$ = Density difference ($slugs\ ft^{-3}$)

τ = Shear stress ($lbs\ ft^{-2}$)

∇^2 = Laplace operator

INDICES:

a = air

b = bottom

c = cold

Cr = critical

g = gate

H = horizontal

i = interface

ℓ = lake or reservoir

o = outlet

s = surface of water

t = total

V = vertical

w = warm

'(prime) = expression using $\frac{\Delta\rho}{\rho}\,g$ instead of g

$\bar{}$(bar) = dimensionless quantity

LIST OF FIGURES

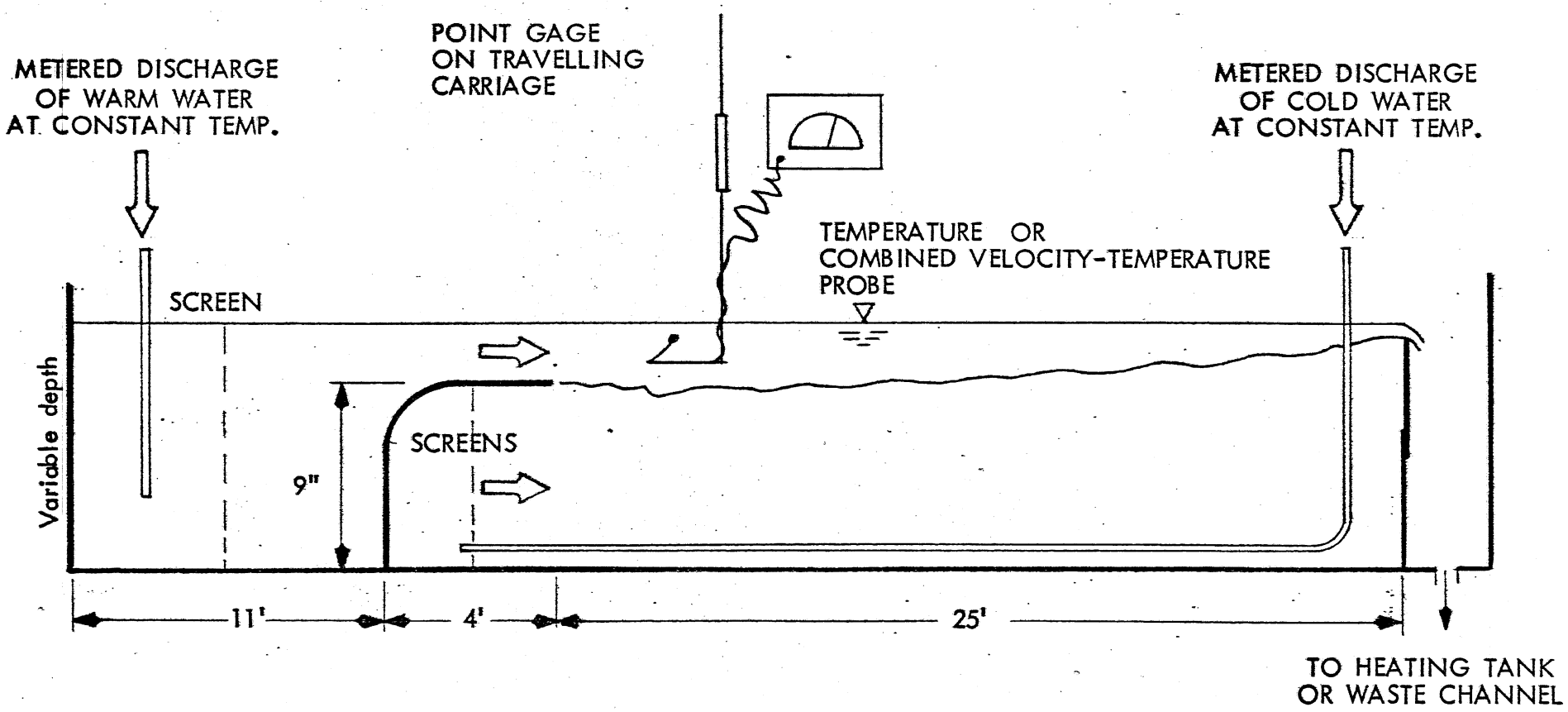

Fig. 1 Two-Dimensional Test Facility Scheme
(Not to Scale)

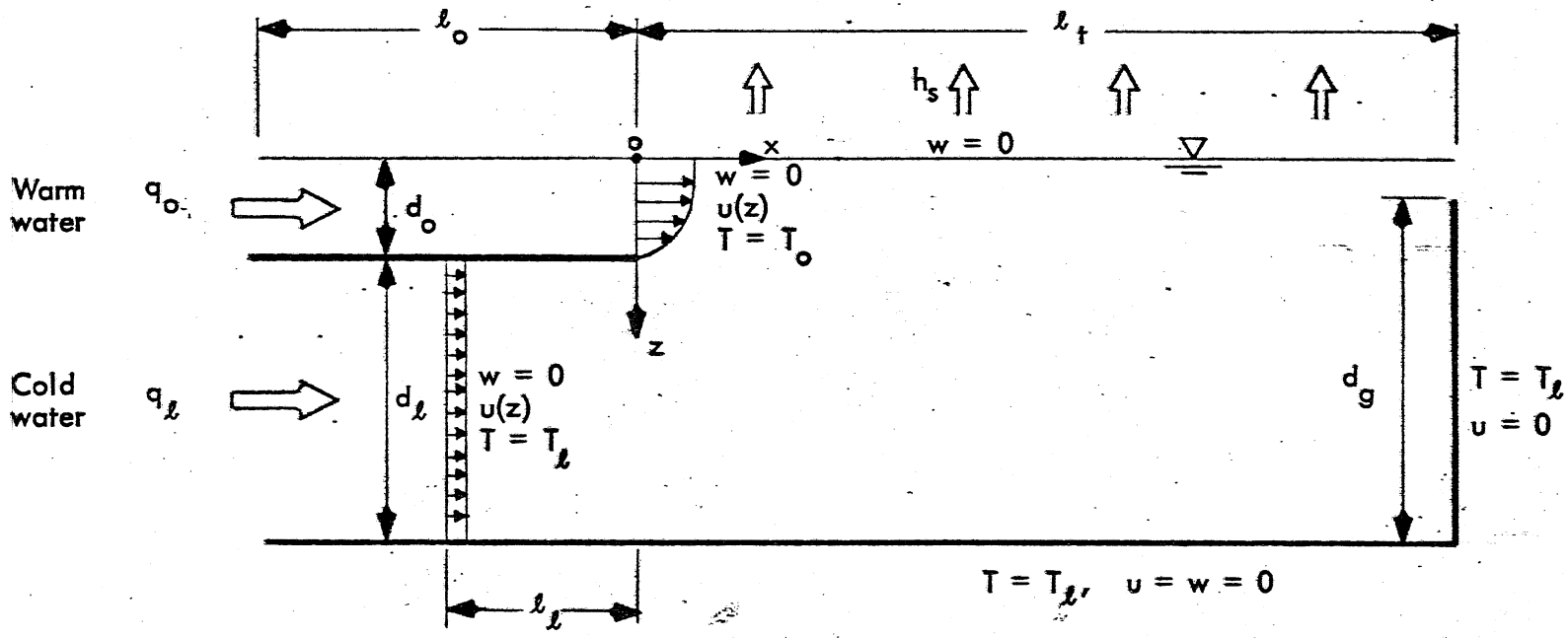

Fig. 2a Schematic of Flow and Boundary Conditions in Flume

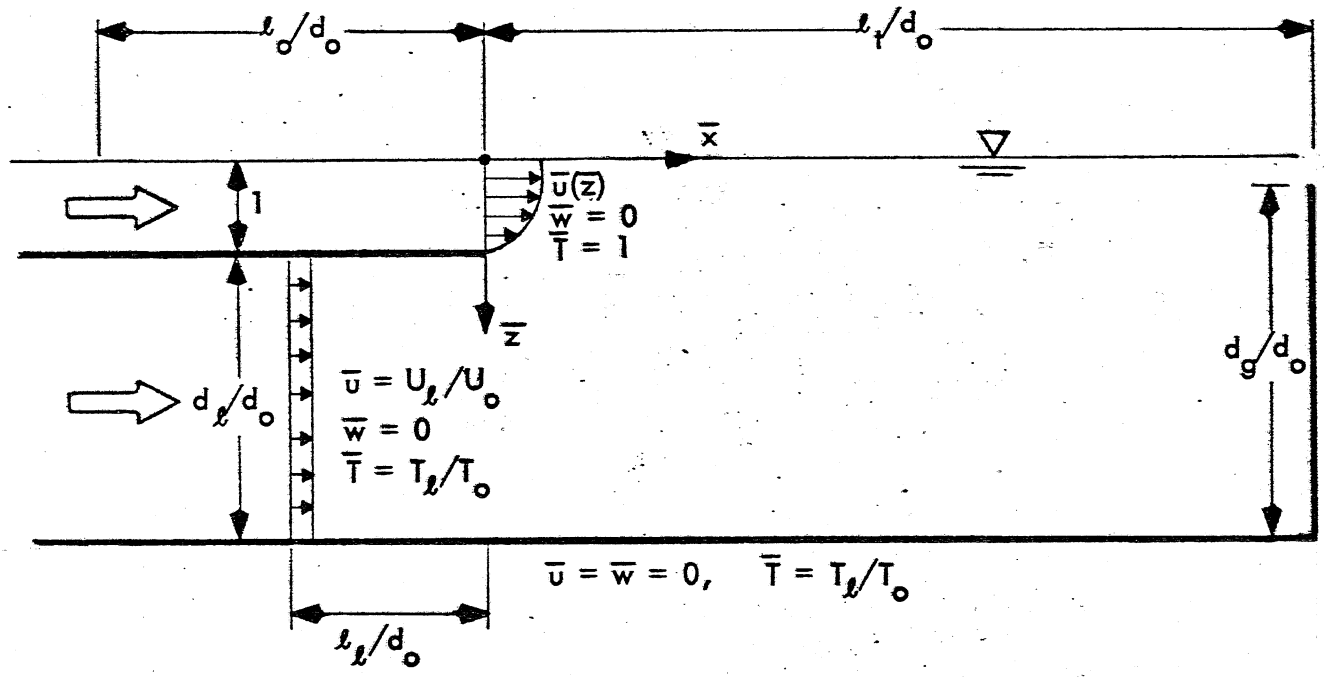

Fig. 2b Schematic of Flow and Dimensionless Boundary Conditions in Flume

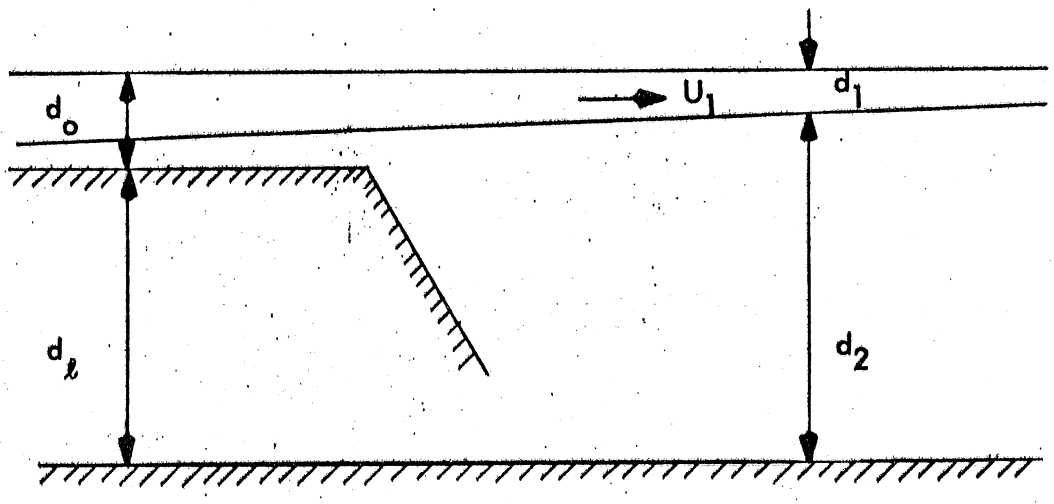

Fig. 3 Two-Layered Stratified Flow System - Cold Water Penetrating into Outlet Channel

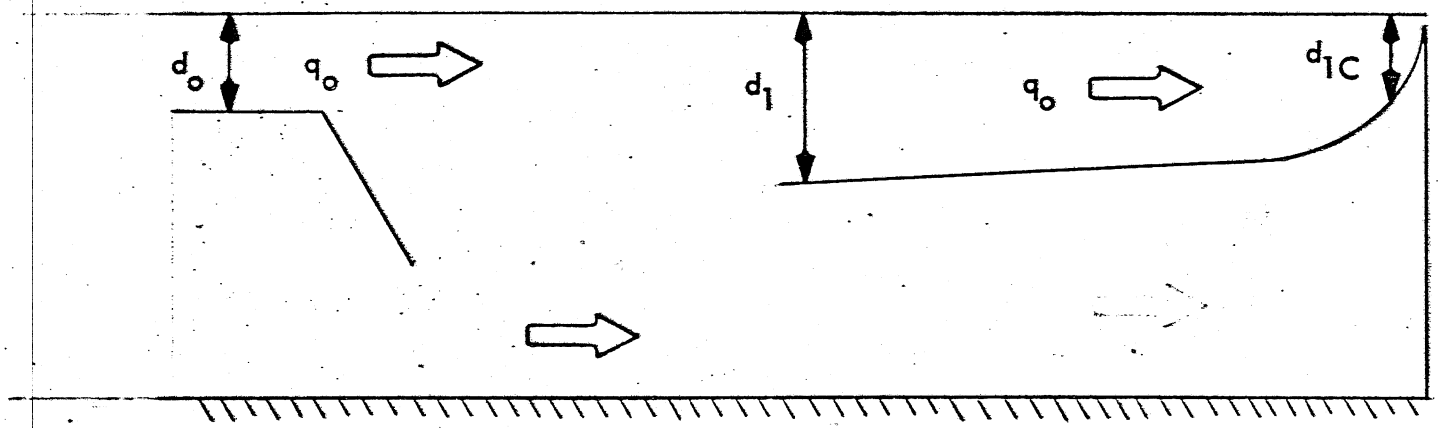

Fig. 5 Tailgate Effect on Flow Near Outlet (No mixing)

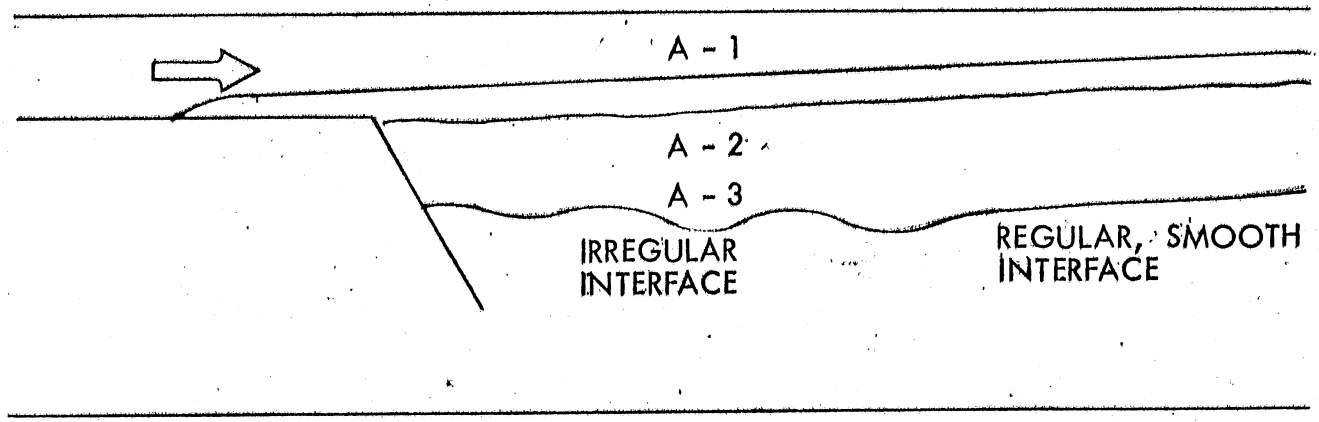

TYPE A-FLOW: STABLE, SMOOTH INTERFACE

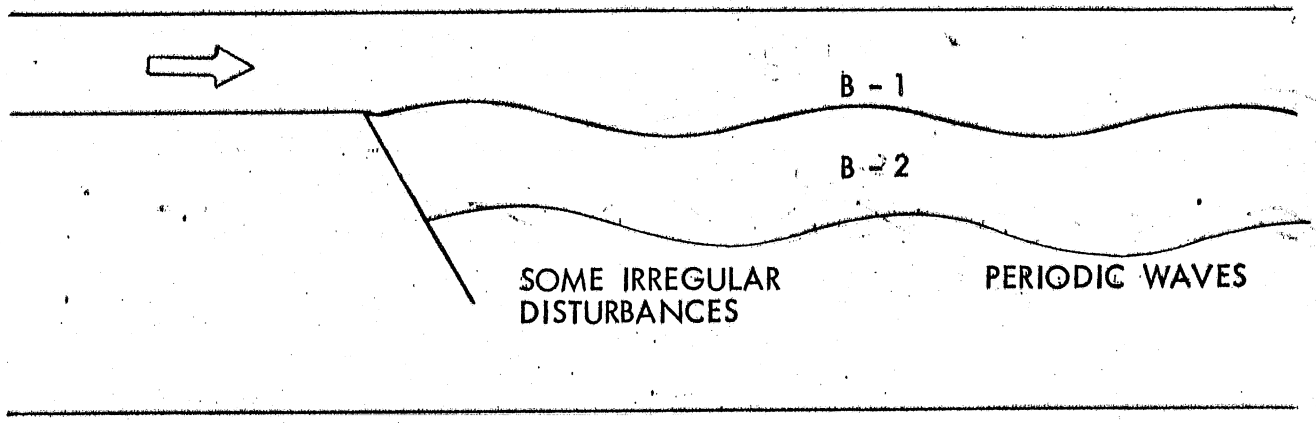

TYPE B-FLOW: PERIODIC INTERFACIAL WAVES

Fig. 6 Schemes of Interfacial Profiles which are Tailgate-Controlled

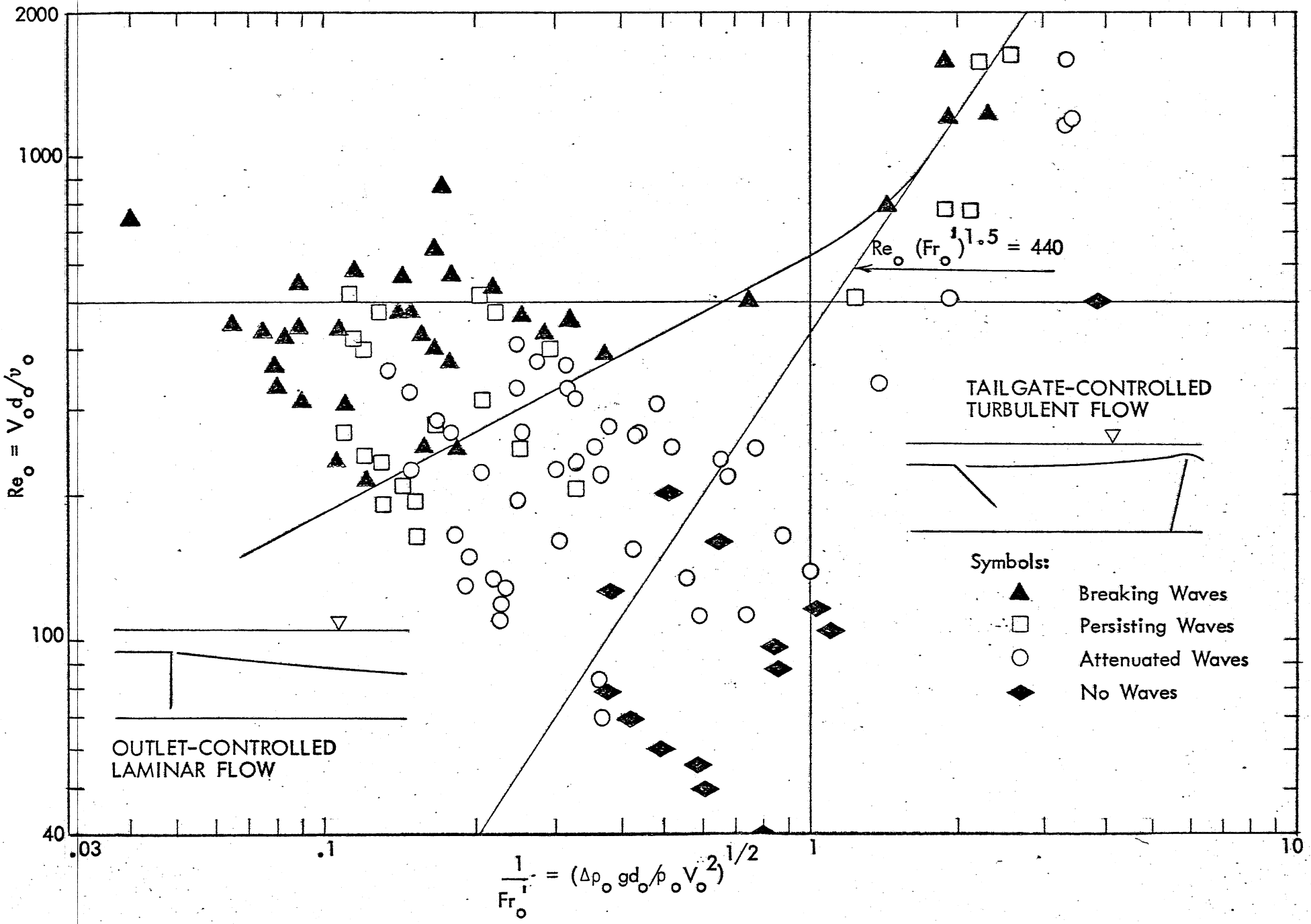

Fig. 7 Experimental Results on Interfacial Waves

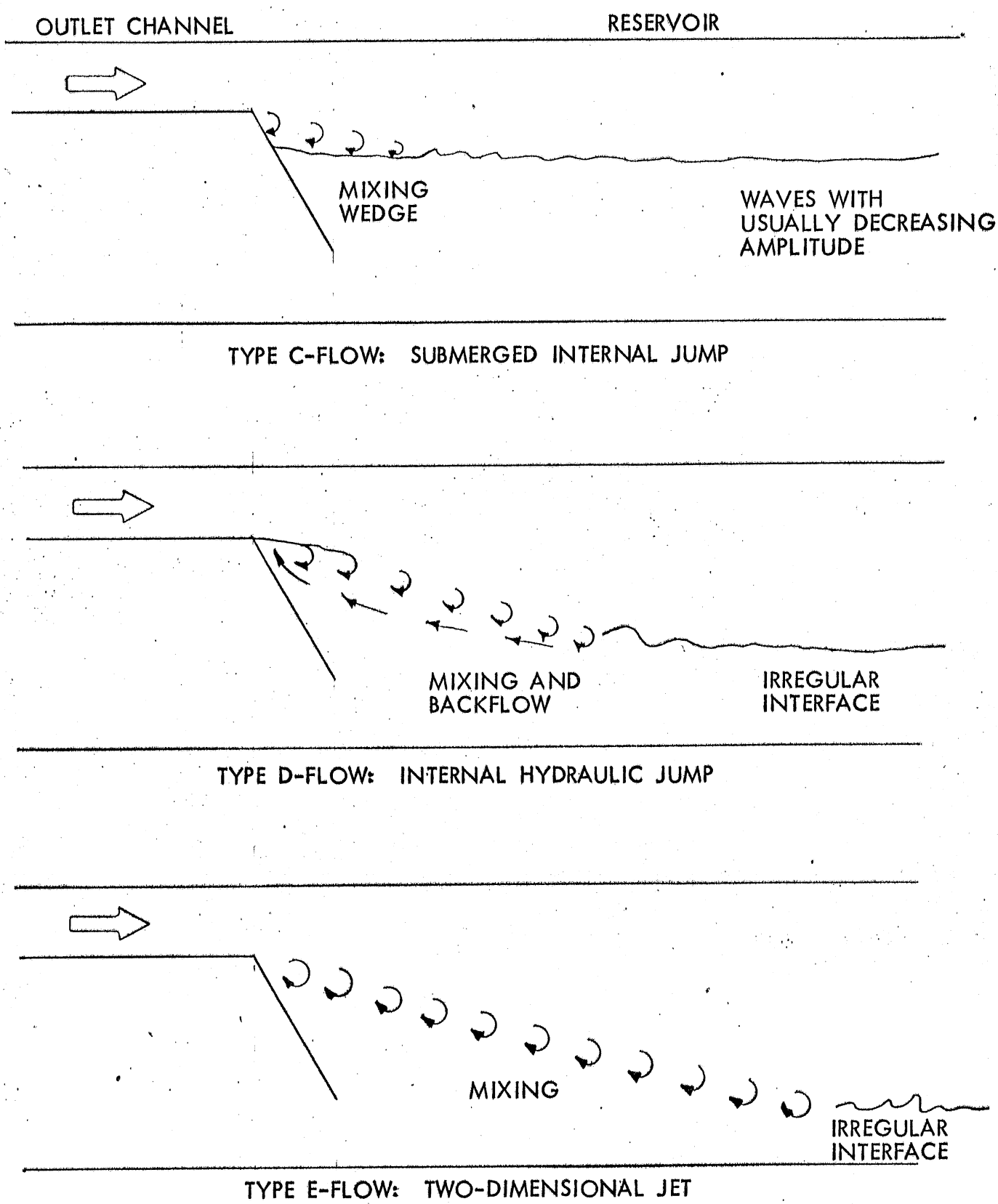

Fig. 8 Schemes of Interfacial Profiles which are Partially or Entirely Outlet-Controlled

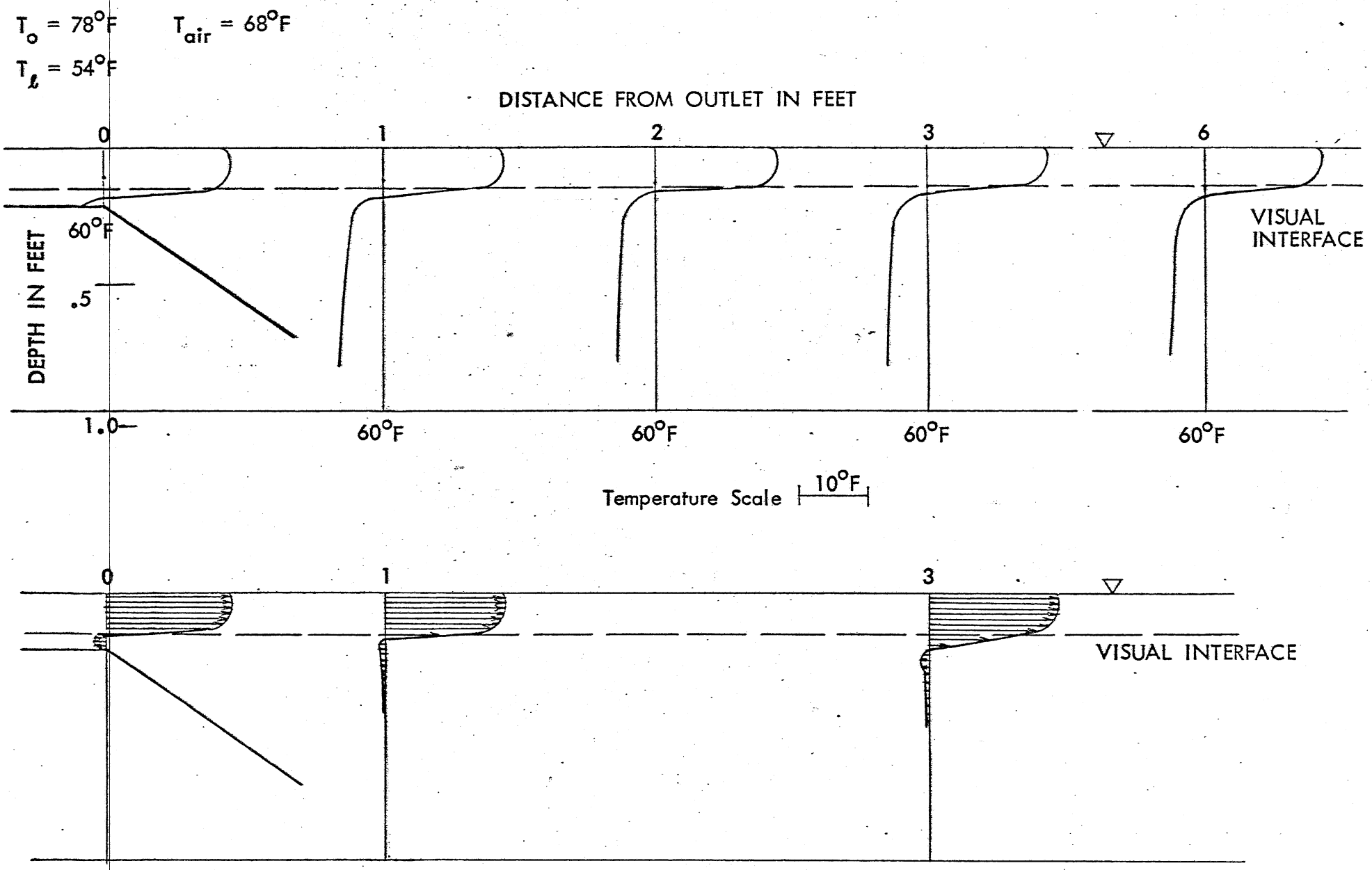

Fig. 9a Measured Temperature and Observed Velocity Distributions Type A-1 Flow. $Fr_o' = 0.29$, $Re_o = 450$, Test 1, 1968

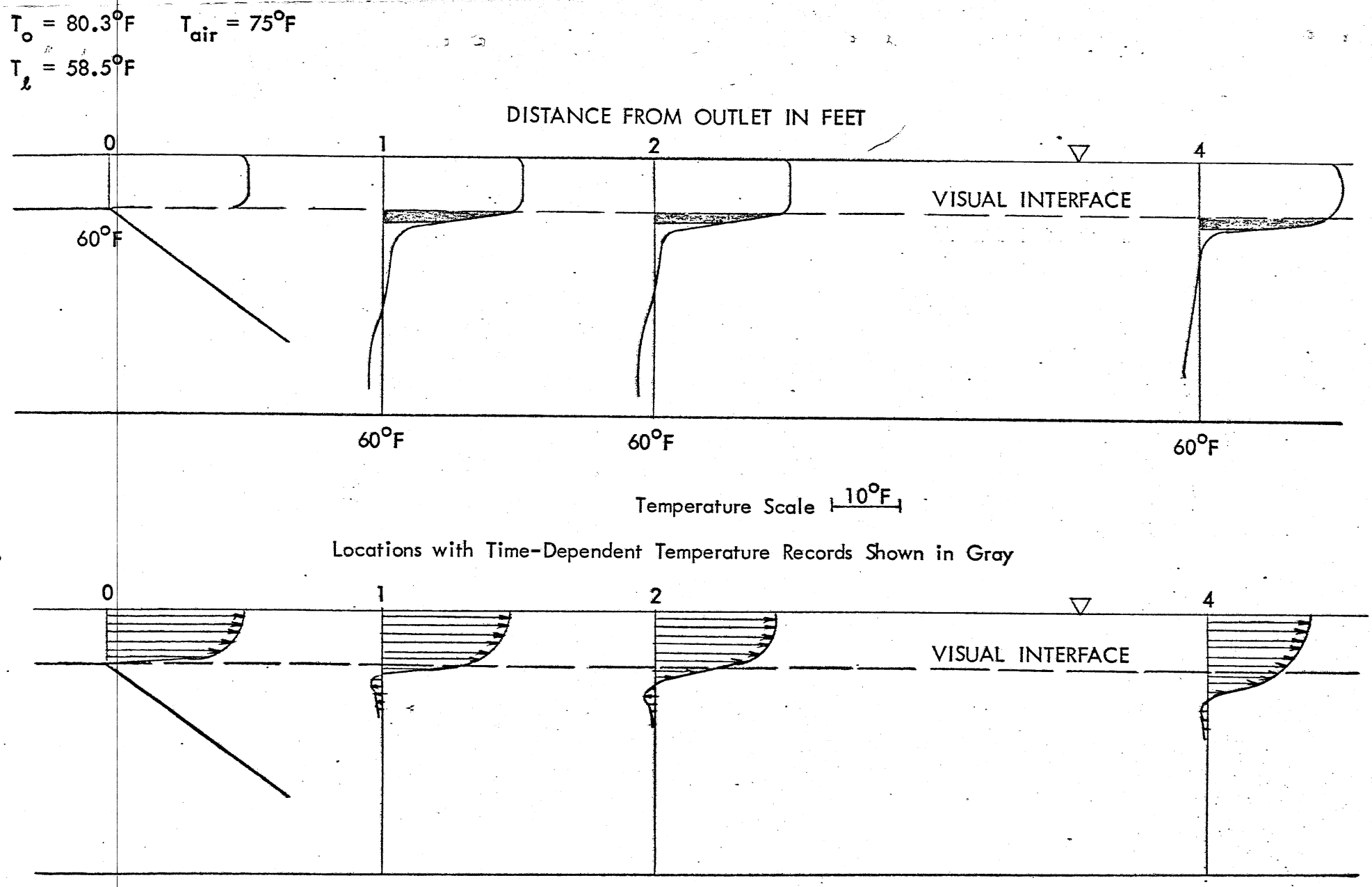

Fig. 9b Measured Temperature and Observed Velocity Distributions
Type A-2 Flow. $Fr_o' = 0.33$, $Re_o = 930$, Test 2, 1968

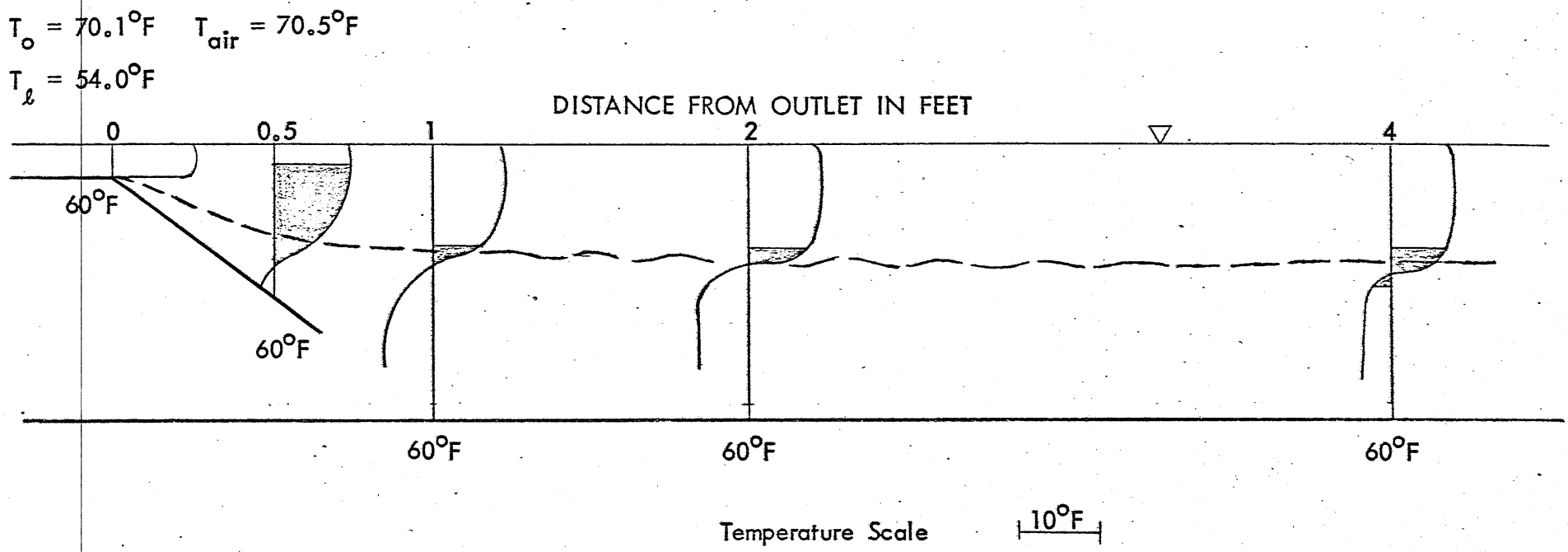

Fig. 9c Measured Temperature Distribution. Type D Flow.
$Fr_o' = 2.0$, $Re_o = 1320$, Test 6, 1968

T_o = 67.8°F T_{air} = 69°F

T_ℓ = 55.0°F

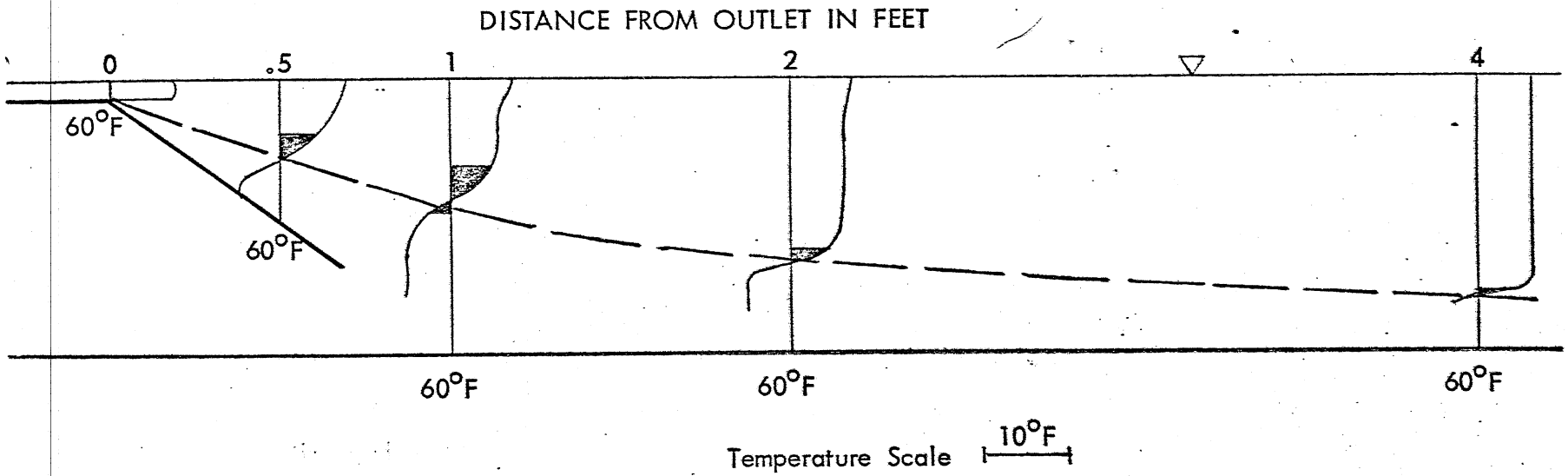

Locations with Time-Dependent Temperature Records Shown in Gray

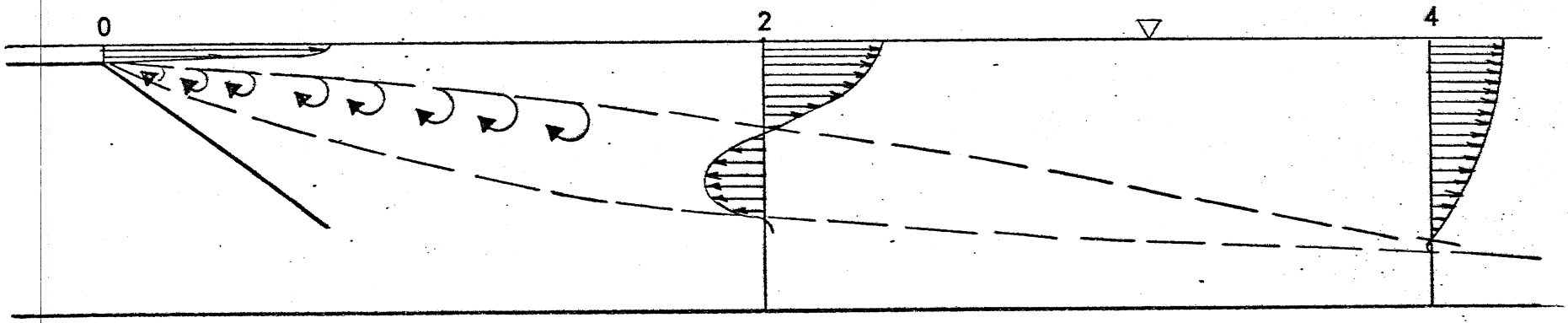

Fig. 9d Measured Temperature and Observed Velocity Distributions
Type D Flow. $Fr_o' = 6.5$, $Re_o = 1420$, Test 4, 1968

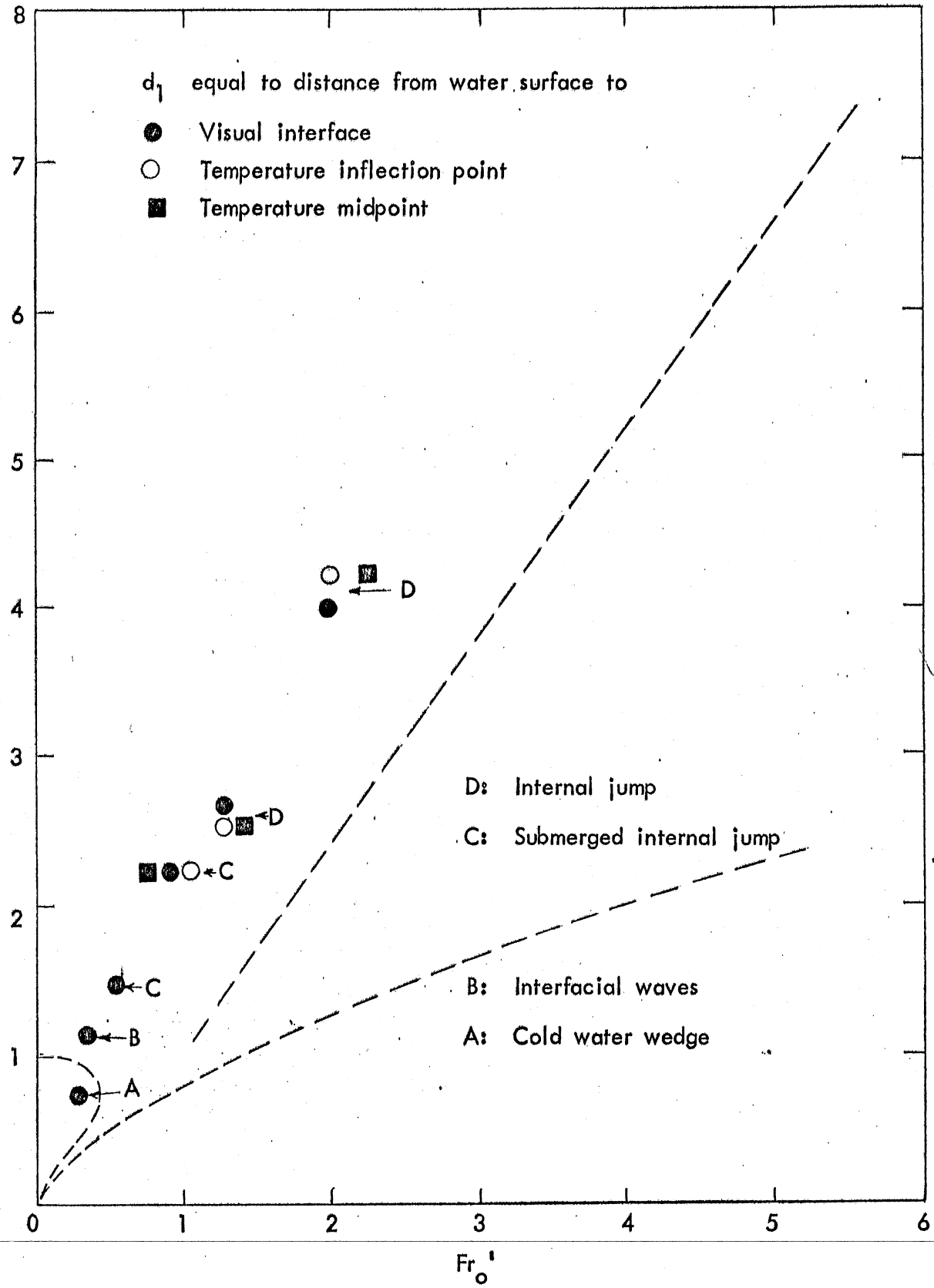

Fig. 10b Depth Ratios Observed at Reynolds Numbers Re_o from 450 to 1550

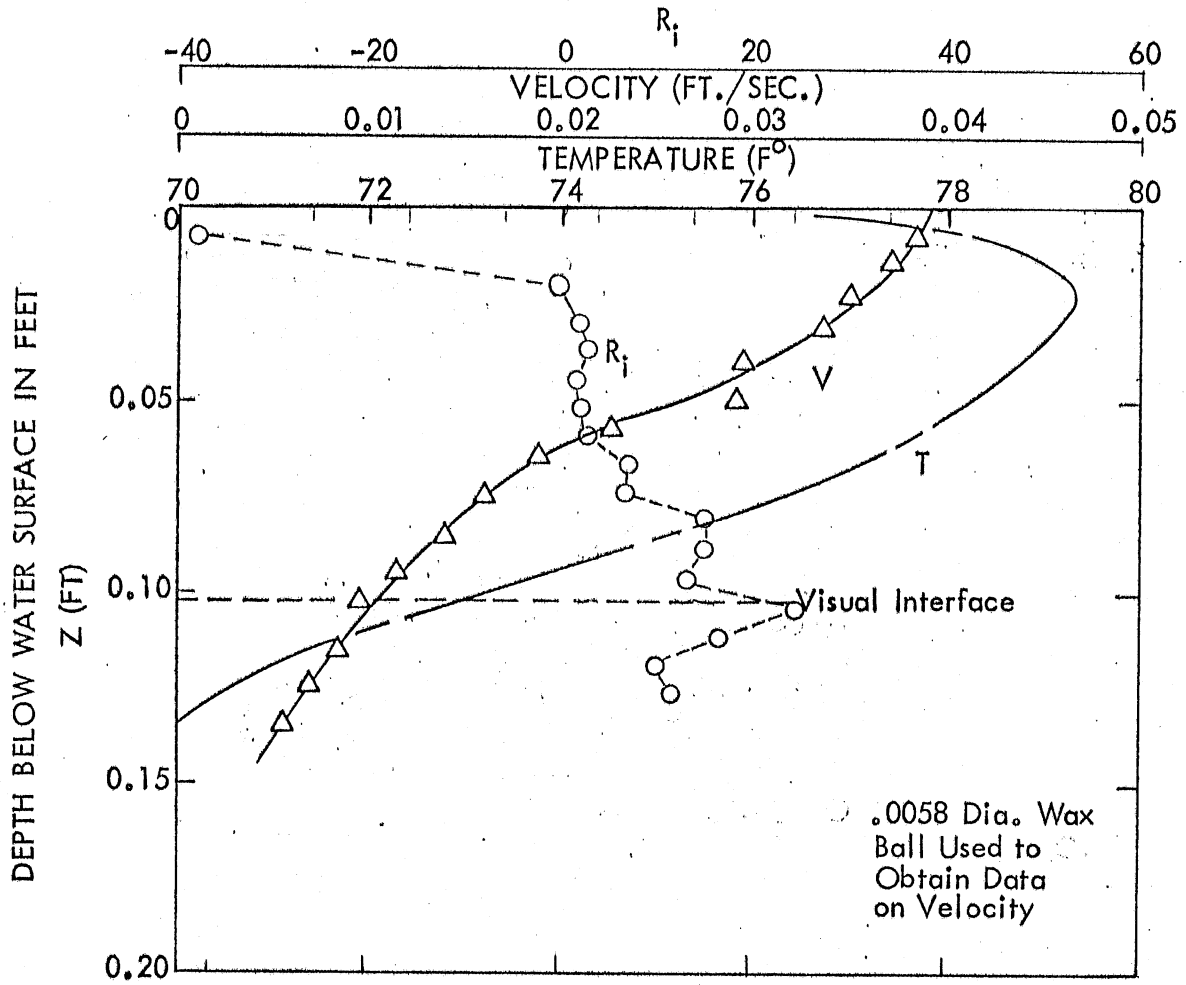

Fig. 11a - TEMPERATURE, VELOCITY AND RICHARDSON NUMBER DISTRIBUTIONS IN THE TWO-DIMENSIONAL WARM WATER SURFACE LAYER

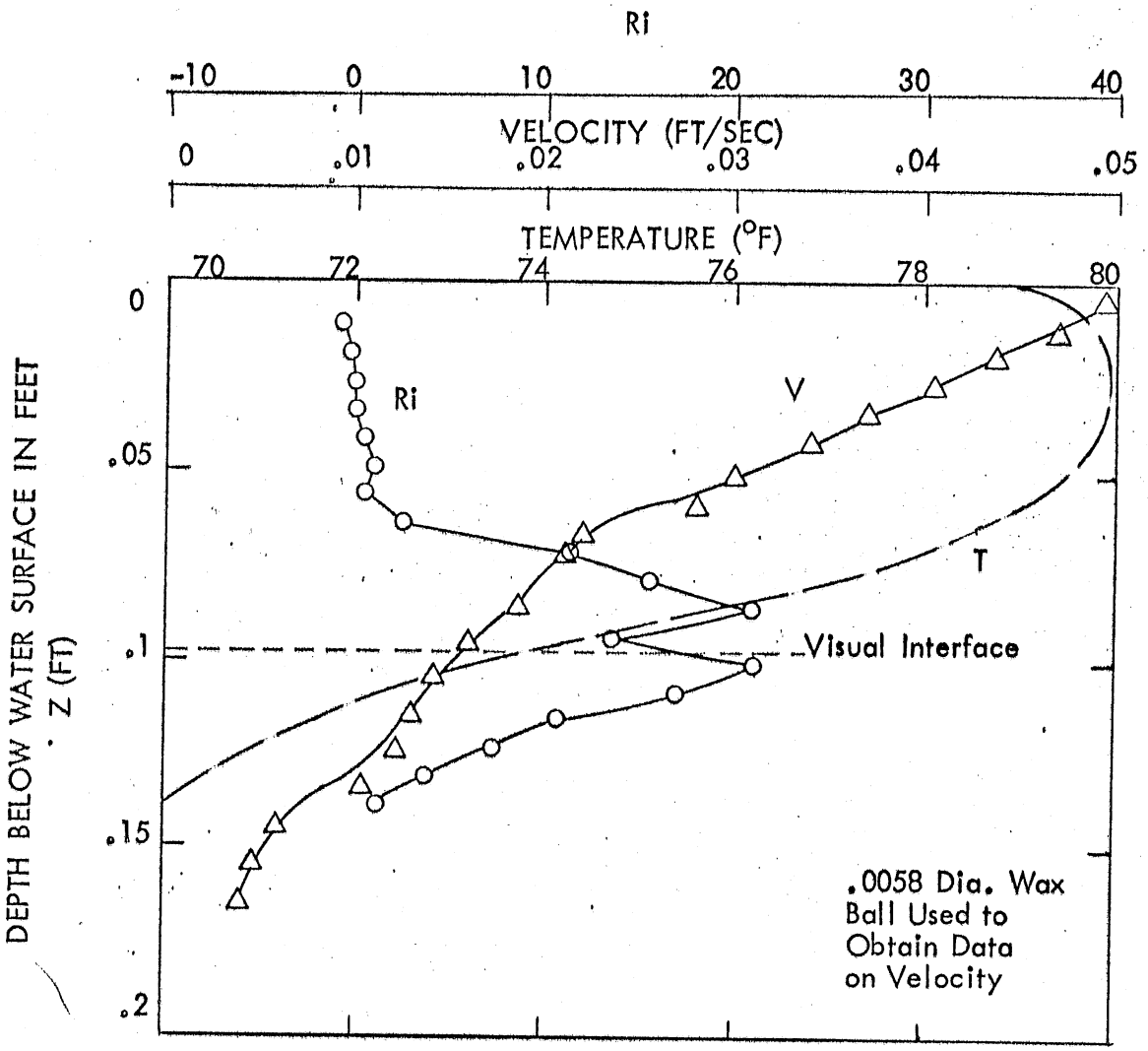

Fig. 11b - TEMPERATURE, VELOCITY AND RICHARDSON NUMBER DISTRIBUTIONS IN THE TWO-DIMENSIONAL WARM WATER SURFACE LAYER

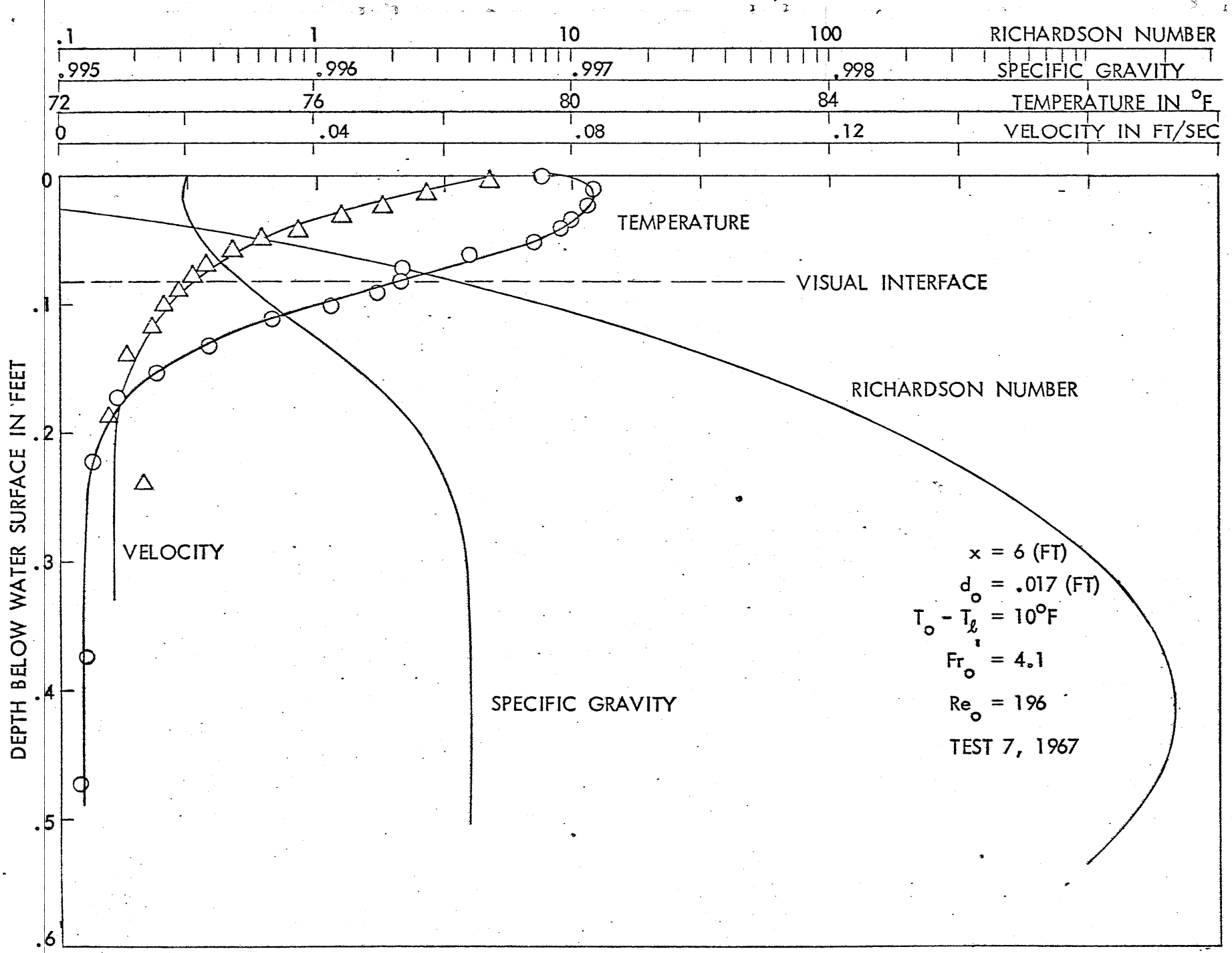

Fig. 11c Temperature, Velocity, Specific Gravity, and Richardson Number Distributions in the Two-Dimensional Warm Water Surface Layer

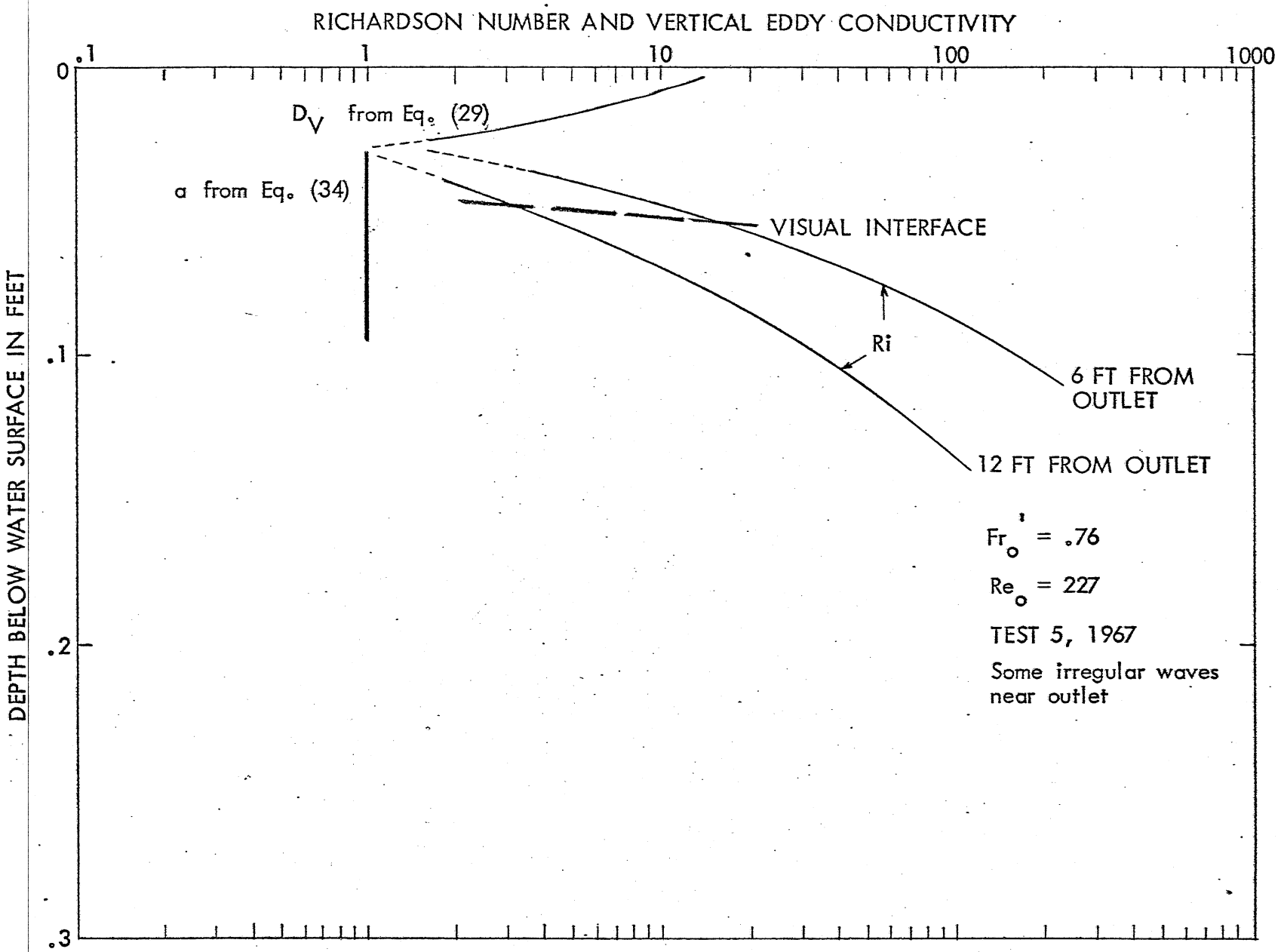

Fig. 12 Distribution of Vertical Eddy Conductivity and Richardson Number in a Particular Test

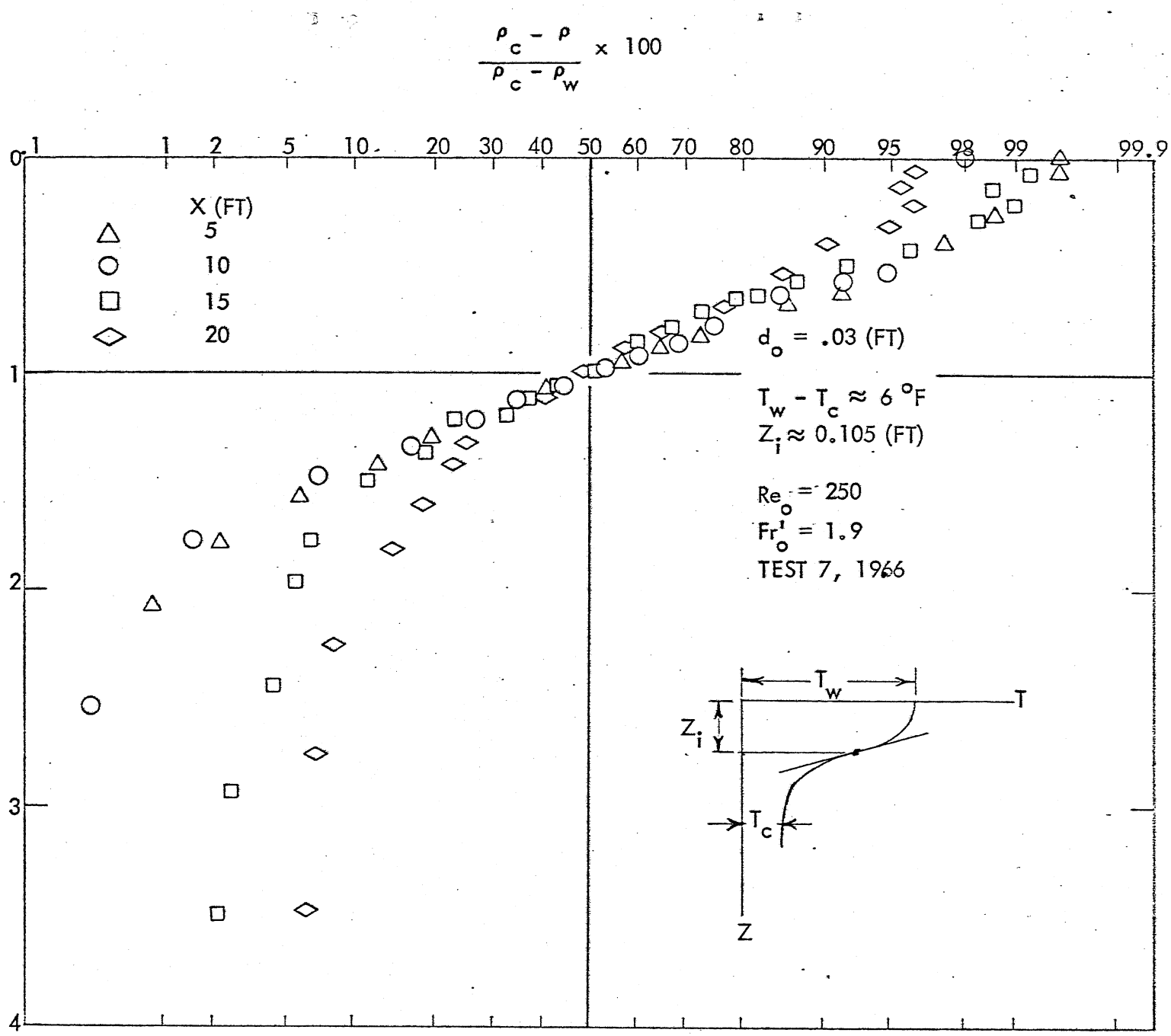

Fig. 13a – DIMENSIONLESS DENSITY DISTRIBUTIONS IN A TWO-DIMENSIONAL MIXING ZONE AT VARIOUS DISTANCES FROM THE OUTLET ON PROBABILITY PAPER

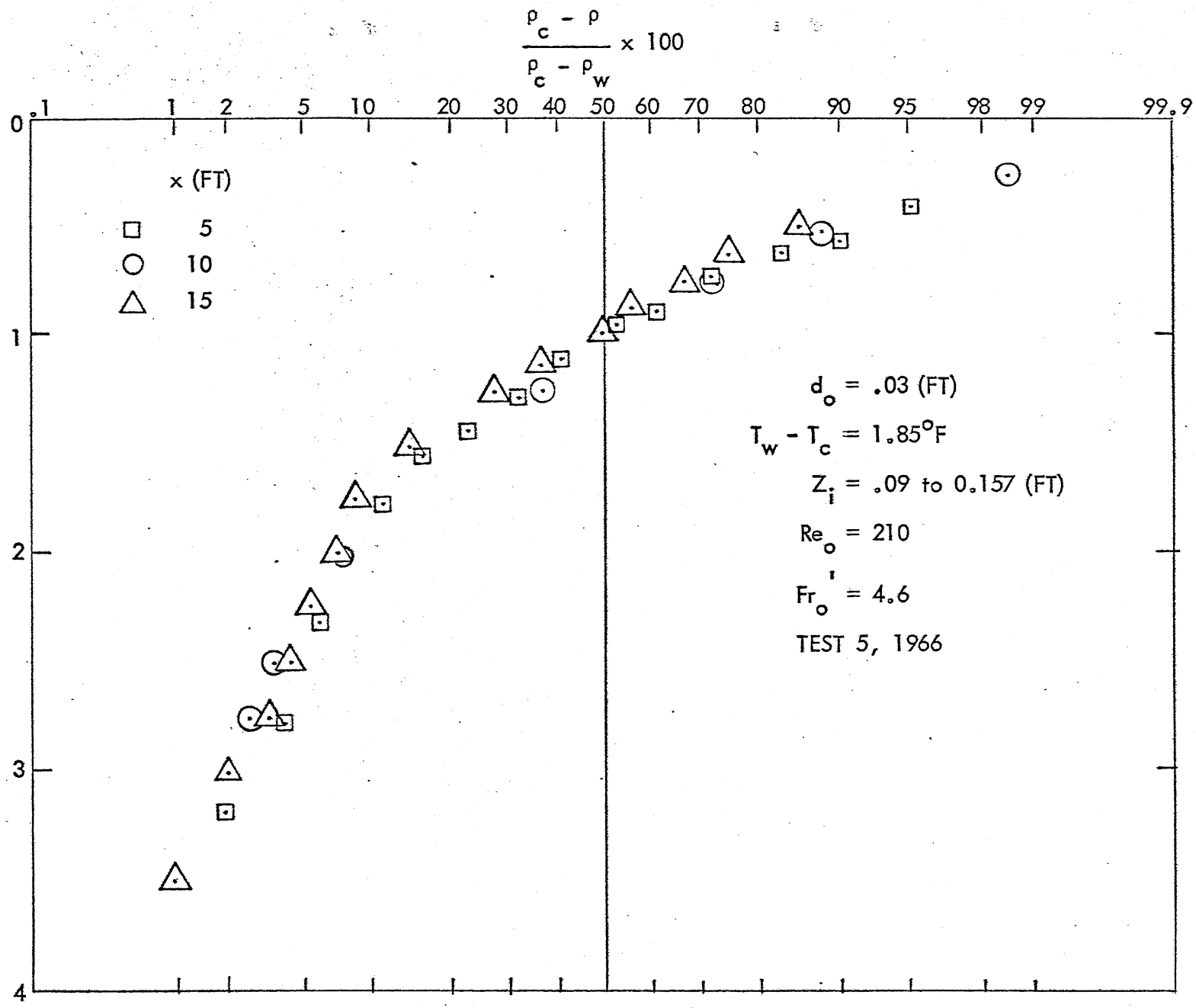

Fig. 13b Dimensionless Density Distribution in a Two-Dimensional Mixing Zone at Various Distances from the Outlet on a Probability Scale

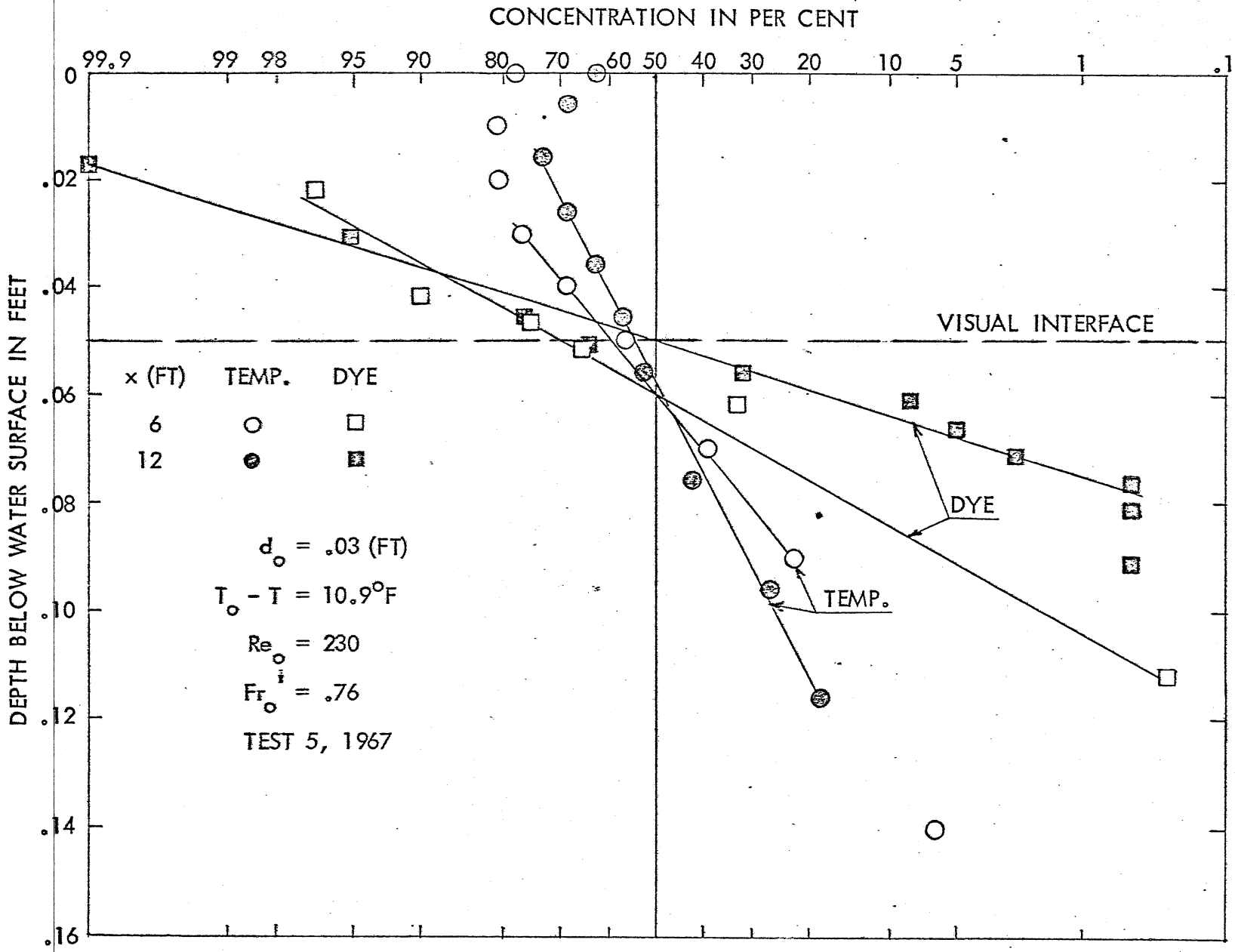

Fig. 14 Comparison of Dimensionless Temperature Differences and Dye Concentrations at 6 ft and 12 ft from the Outlet. Values at Outlet are Used as References.

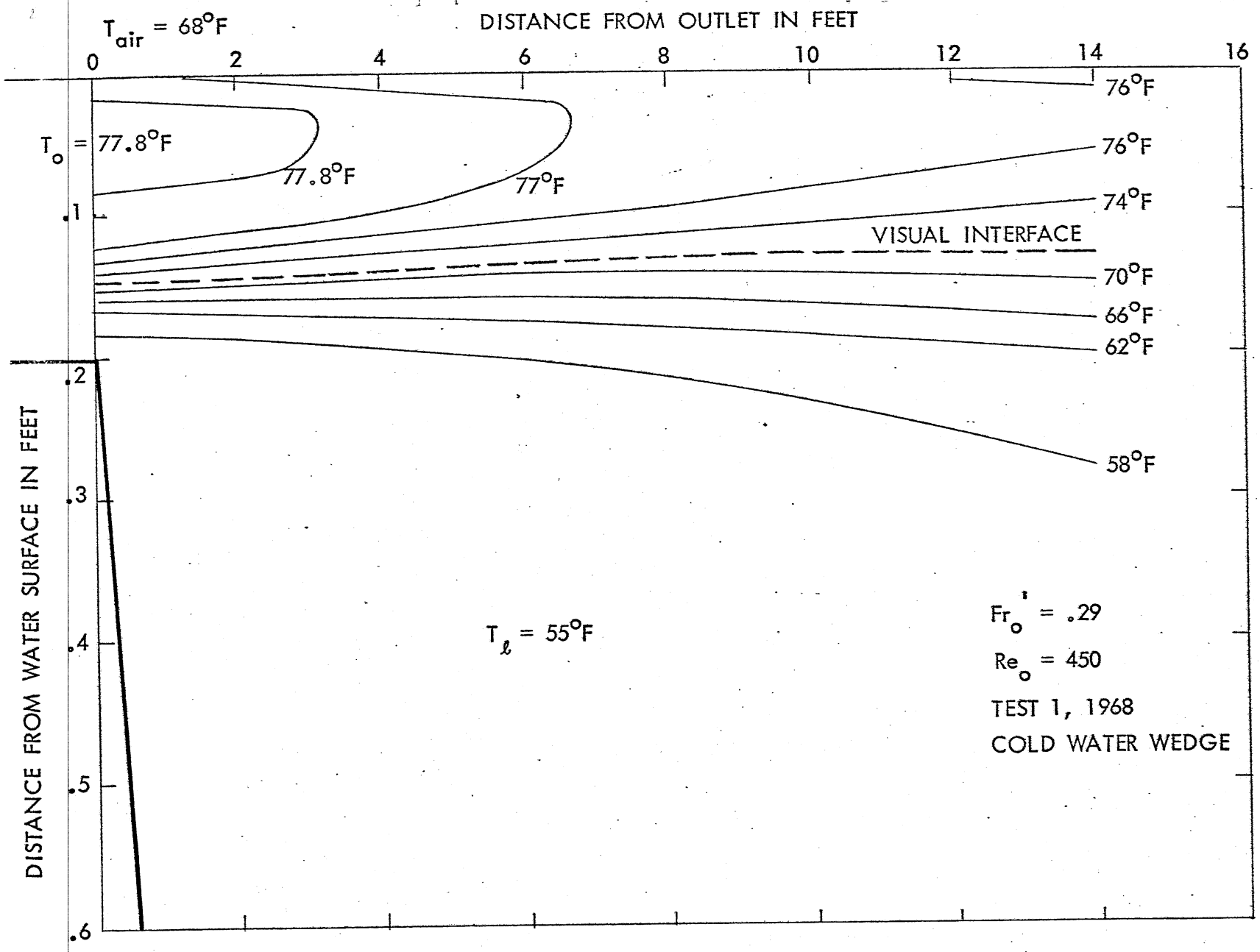

Fig. 15a Isotherms near Outlet - Type A-1 Flow

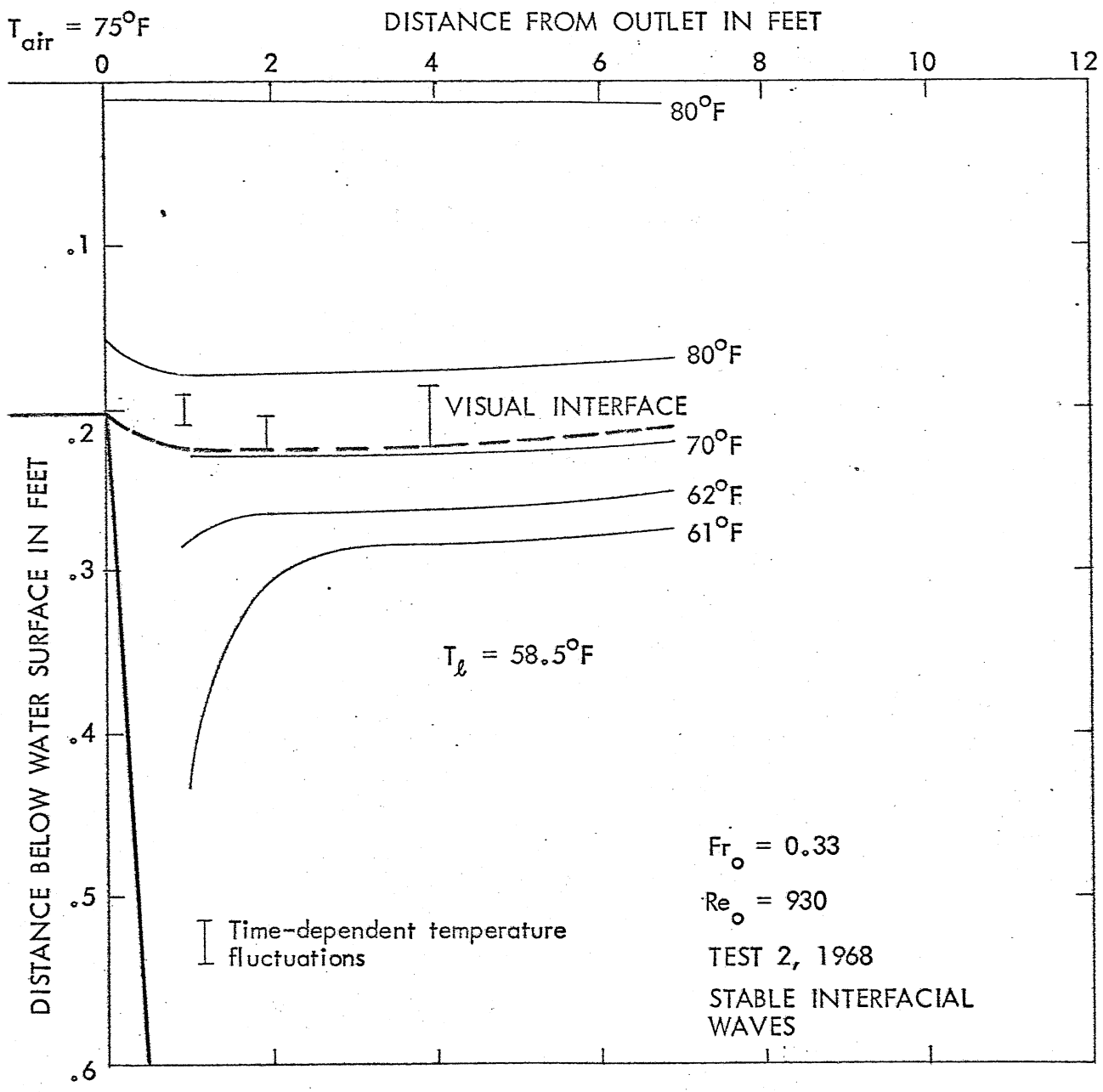

Fig. 15b Isotherms near Outlet - Type A-2 Flow

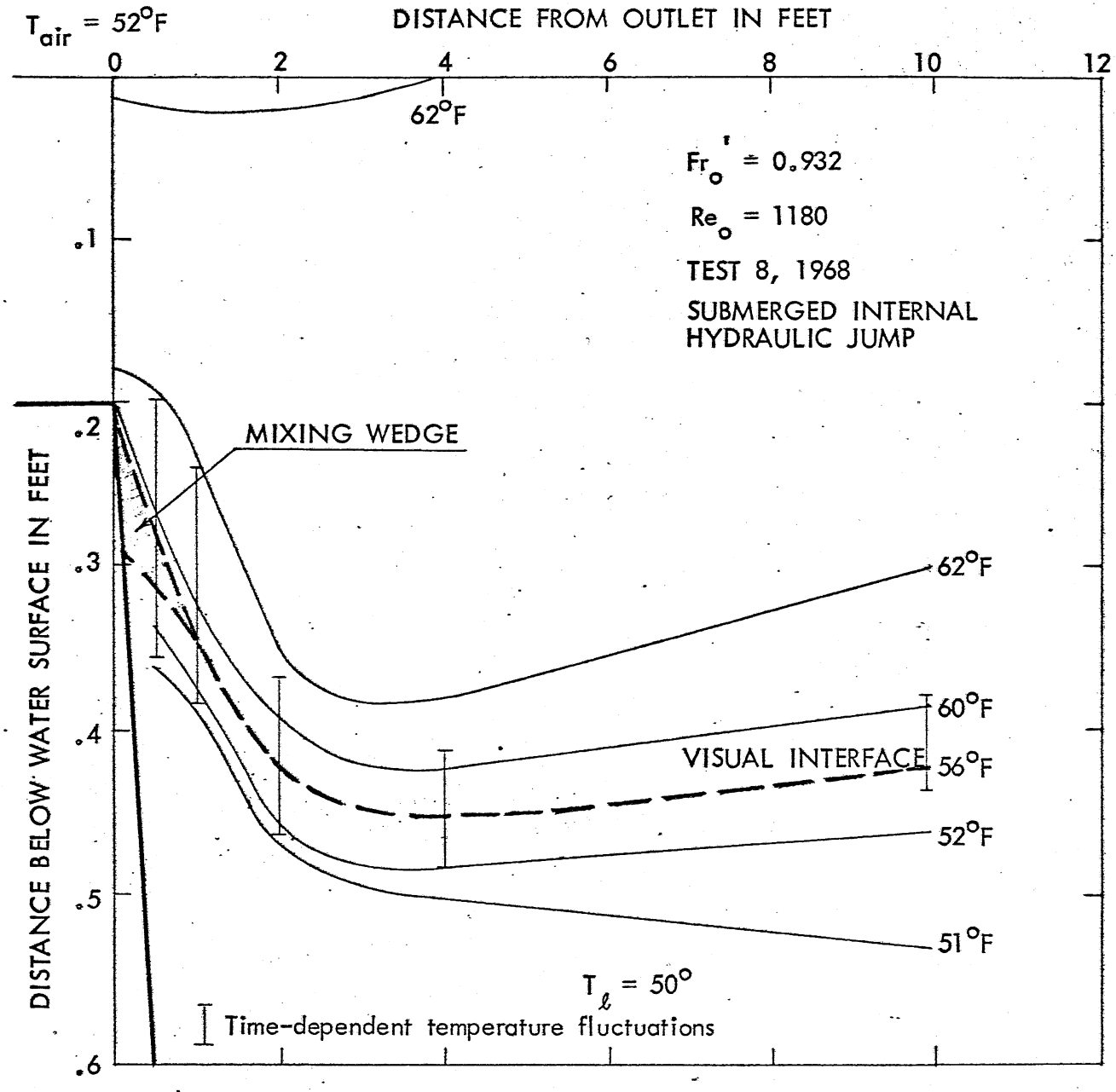

Fig. 15c Isotherms near Outlet - Type C Flow

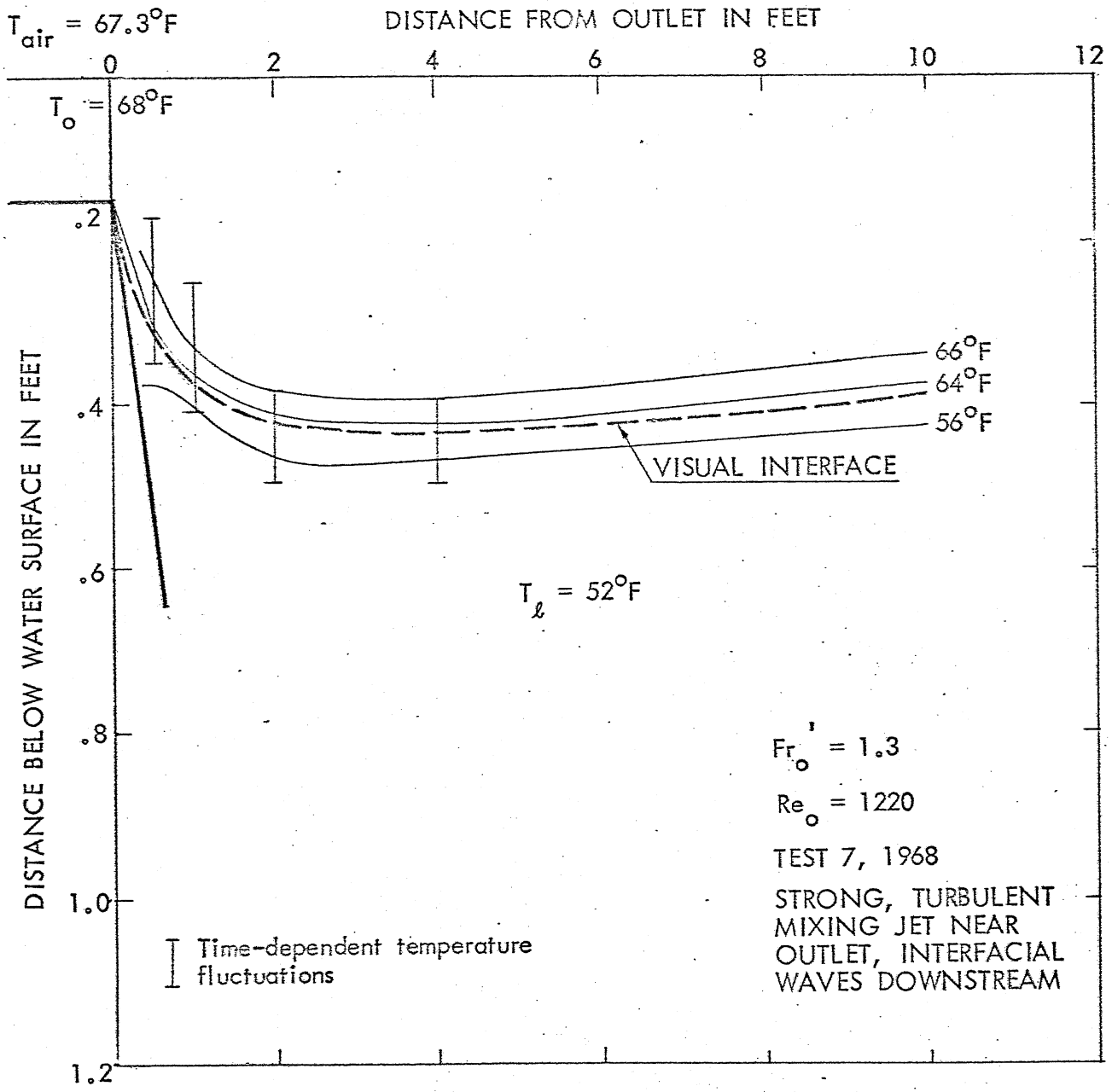

Fig. 15d Isotherms near Outlet - Type D Flow

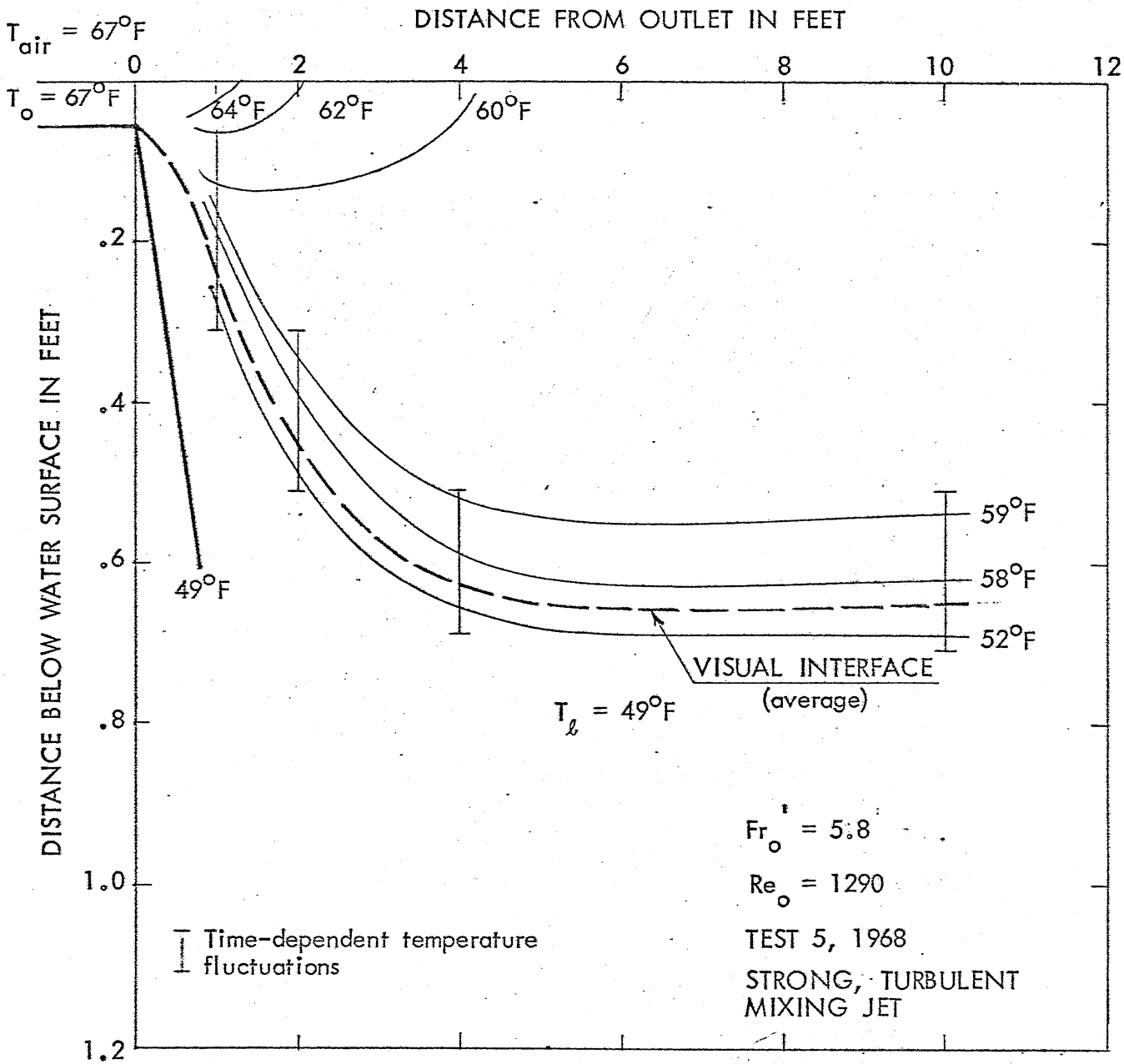

Fig. 15e Isotherms near Outlet - Type D Flow

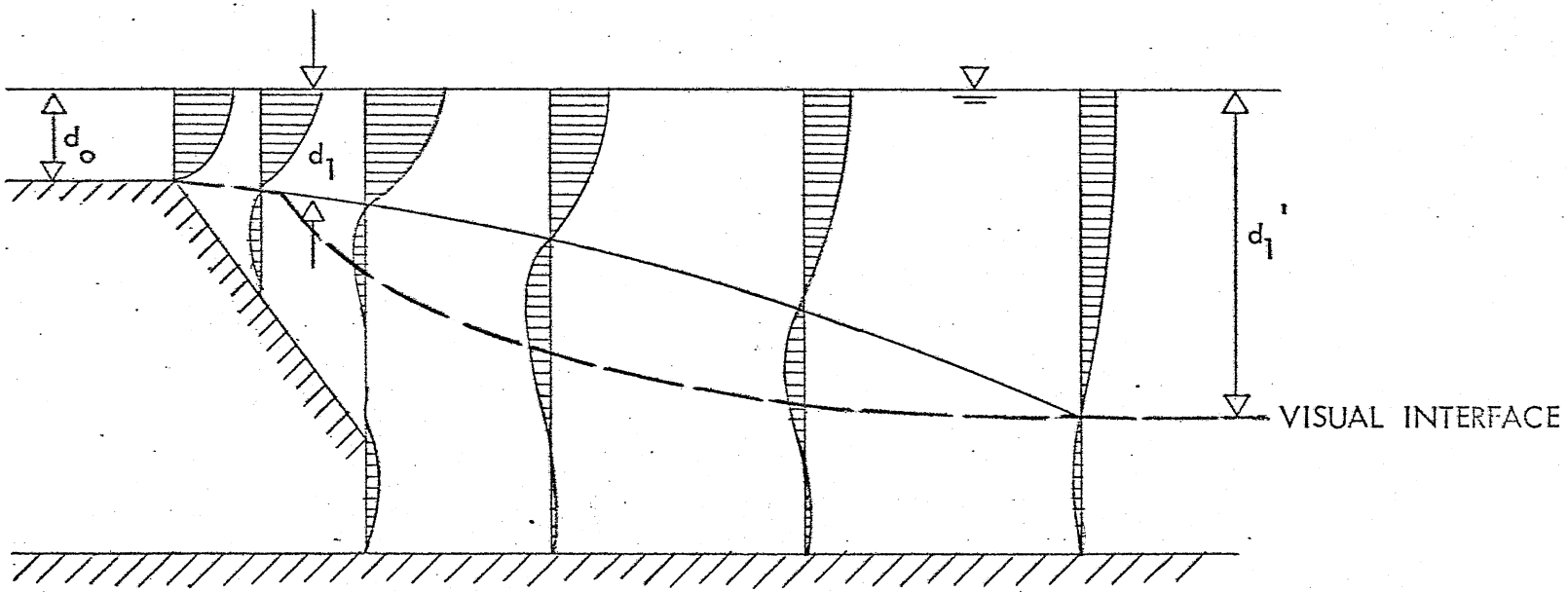

Fig. 16 Schematic of Two-Dimensional Buoyant Jet Indicating Qualitatively Velocity Distributions, Visual Interface, and Conjugate Depths

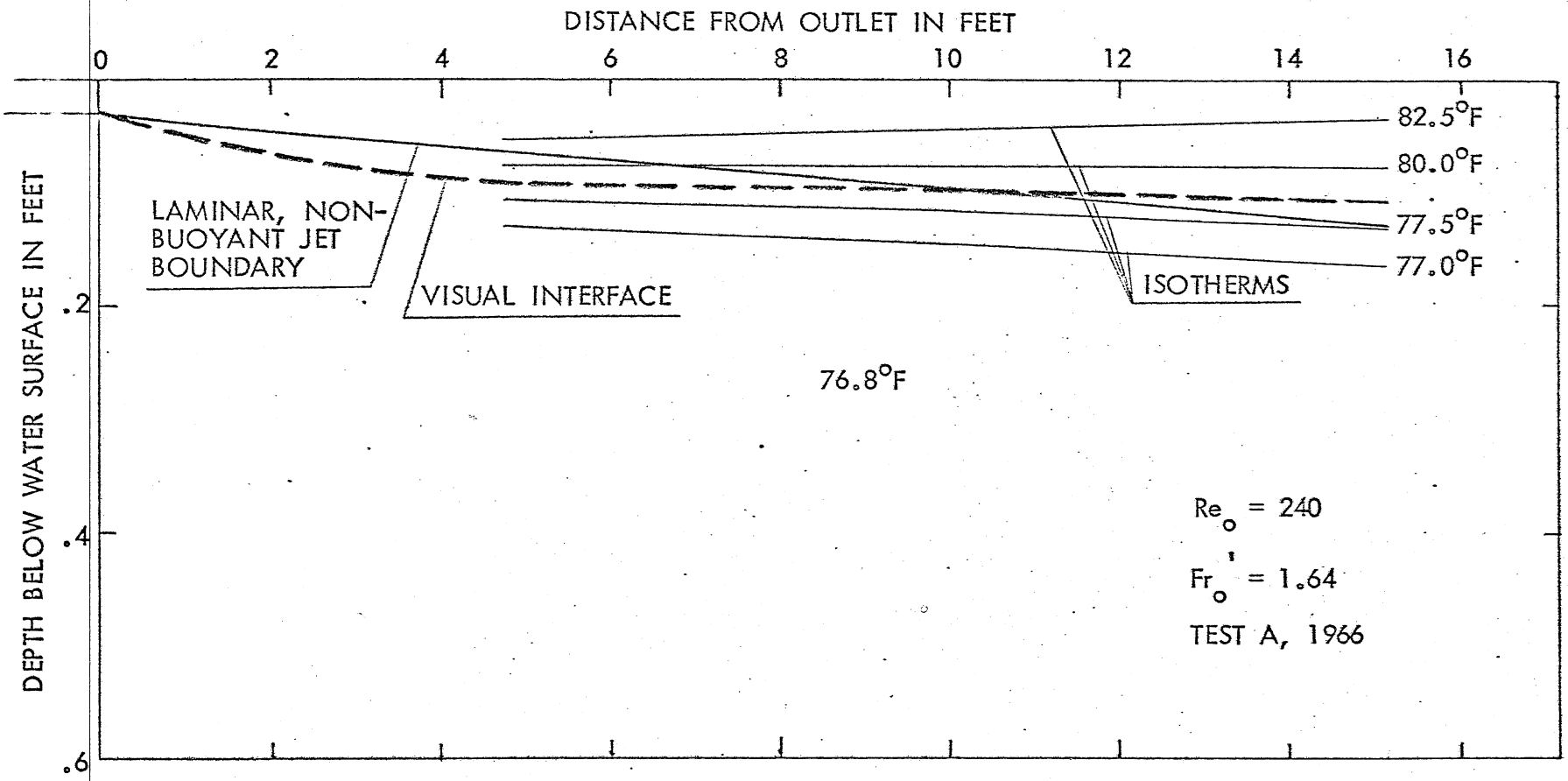

Fig. 17 Comparison of Experimental Isotherms and Visual Interface with Two-Dimensional, Non-Buoyant, Laminar Jet Theory

APPENDIX A

HEAT TRANSFER AT THE AIR-WATER INTERFACE

The experiments were carried out in a flume mounted in approximately the center of a larger laboratory floor. There was no noticeable air draft in the room, and the walls of the flume, extending several inches above the water surface, also prevented the formation of air currents over the water surface. It appears to be a fairly sound assumption that air temperature and humidity were constant along the total length of the flume.

The exchange of heat across the air-water interface is rather complex because it is the sum of radiation, evaporation, convection, and conduction processes. Reference [3] is one of numerous publications dealing with this problem.

The value of the surface heat conductance can be either calculated or measured. Relationships of the kind presented in Reference [3] can be used for calculations. In the present case this method is not useful, however, because not all required input variables are known.

Measurements on natural lakes show that the average surface coefficient of heat transfer is ordinarily in the range from 50 to 200 BTU ft^{-2} day^{-1} $^{o}F^{-1}$ over a wind speed range from 2 to 10 mph (Reference [3]). A value near the upper limit was used in a study of a power plant on Lake St. Croix reported on in Reference [4]. Similar values are likely to be found in the laboratory. With the absence of wind and the high air humidity in the summer, laboratory values are probably at the lower end of the range cited, whereas the drier air found during the winter will raise the value of the coefficient.

APPENDIX B

ANTICIPATED QUALITATIVE EFFECTS OF SURFACE COOLING, CONDUCTION, AND CONVECTION ON WATER TEMPERATURES IN THE WARM WATER LAYER

For the purpose of this discussion the warm water layer may first be compared to a slab of thickness d_o subjected to surface cooling. Under these circumstances a Biot modulus $d_o k_s/k$ of less than 0.1 signifies, according to Reference [5], page 139, that a very small temperature gradient within the slab is necessary to provide the necessary heat flux to the surface from which the heat is dissipated. The internal resistance to heat flow is insignificant compared to the surface resistance.

In the experiments carried out the Biot modulus is larger than 0.1, indicating that a temperature gradient across the depth must develop if the heat dissipated on the water surface is transported from the interior of the fluid to the interface by conduction alone. This is not the case, however, because convective heat transfer actually takes place.

In order to check the relative importance of convection as compared to surface heat loss to the atmosphere, the flow in the channel before the outlet may be considered. The heat flow model assumes that the heat lost at the water surface is all coming from the bottom of the channel, to which the convective coefficient k_{sc} applies. In reality the heat is already contained in the fluid and does not have to traverse the whole layer of thickness d_o.

The ratio of the convective heat transfer coefficient D_v to the conductive heat transfer coefficient k is

$$\frac{D_v}{k} = \frac{Nu_o}{d_o}$$

The Nusselt number is a function of Reynolds and Prandtl numbers:

$$Nu_o = f(Re_o, Pr_o)$$

and replaces the Biot modulus if the heat exchange takes place by convection rather than conduction. For open channel flow, where heat is lost at the water surface and the channel bottom may be assumed to be insulated, the relationship between Nu_o and Re_o is not readily available in the literature.

Instead, information on convective heat transfer from a solid surface to a fluid flowing parallel over it is used. A free surface and a solid wall can be considered to be equivalent with respect to the heat transfer problem; however, they do influence the velocity distribution and turbulence in substantially different ways. Therefore the analogy can be expected to give only a very rough estimate.

In laminar flow, according to Reference [5], p. 296, the local convective surface heat transfer coefficient at a distance x from the leading edge of a flat plate is

$$k_{sc} = 0.322 \frac{k}{x} Re_x^{.50} Pr^{.33}$$

If point x is supposed to coincide with the outlet, then x is the length of plate required to give a fully developed velocity profile over a depth d_o.

The relationship between the thickness of the boundary layer δ and the distance from the leading edge in laminar flow over a flat plate is

$$\frac{\delta}{x} = \frac{d_o}{x} = \frac{4.91}{Re_x^{.5}}$$

Therefore x may be replaced in the above equation, which becomes

$$\frac{k_{sc}}{k} = 0.332 \frac{4.91}{d_o} Pr_o^{.33} = 1.63 \frac{Pr_o^{.33}}{d_o}$$

$$\frac{k_{sc}}{k} \approx \frac{Dv}{k}$$

The range of Dv/k values for the laminar flow flume experiments under consideration would be of the order of 10 to 100. The Nusselt number for this type of flow is equal to $Nu_o = 1.63$, and $Pr_o^{.33}$ has a numerical value close to 3.

Since this Nusselt number has about the same order of magnitude as the Biot modulus for surface heat transfer, it is, in conclusion, likely that the

surface heat loss will cause a temperature gradient with distance from the water surface if the flow is laminar.

For Reynolds numbers at the outlet larger than approximately 500, convective heat transfer in turbulent flow over a flat plate must be considered. The local Nusselt number for this type of flow, according to Reference [5], page 313, is

$$Nu_x = 0.0288\ Pr_x^{.33}\ Re_x^{.8}$$

The relationship between the distance x and the depth at the outlet in turbulent flow is

$$\frac{\delta}{x} = \frac{d_o}{x} = \frac{0.371}{Re_x^{.2}}$$

and the local and outlet Reynolds numbers are related by

$$\frac{Re_x}{Re_o} = \frac{x}{d_o}$$

The outlet Nusselt number, therefore, is

$$Nu_o = 0.0775\ Pr_o^{.33}\ Re_o$$

For $Re_o = 500$ the numerical value of Nu_o is of the order of 70, which is a minimum. The maximum will be above 200.

The ratio of the surface heat conductance coefficient to the coefficient of convective heat transfer in turbulent flow is equal to Bi_o/Nu_o and was less than 0.06 in the flume experiments undertaken. The surface heat transport process will therefore very likely not affect the temperature distribution in a vertical cross section through a warm water outlet if the flow is turbulent. Temperatures can be expected to be nearly constant. The result can with fairly good justification be extended to the turbulent warm water layer along the total length of the flume. Temperatures are constant in a cross section, but may decrease with distance from the outlet.

In conclusion, it may be said that the internal resistance of the experimental warm water layer to heat transport may be expected to be small in

turbulent flow. The surface heat loss will likely not affect the experimental temperature distribution in a vertical cross section. In laminar flow, however, surface heat loss must be expected to have an effect. Experimental isotherms for the various outlet flow conditions presented in the main body of this report verify the qualitative expectations expressed in this appendix.

APPENDIX C

GENERAL OBSERVATIONS ON MIXING BETWEEN PARALLEL LAYERS OF DIFFERENT TEMPERATURES IN TURBULENT FLOW

There are, theoretically at least, two types of mixing processes. In one type, interfacial mass exchange is very strong and produces a mixed zone which replaces the interface. Such a process may be called "exchange-controlled." An example would be mixing by strong eddies at the outlet. Turbulence is strong at the outlet, but because of the damping effect of a density gradient (caused by a temperature gradient) the intermediate layer, with intermediate and rather homogeneous temperature and density, can exist over a long distance downstream. It will be limited by two interfaces which will appear more and more clearly as the flow goes on. Eventually they will become unstable, and more mixing will take place, with the formation of additional layers also possible. The existence of such multilayered systems is typical in large bodies of water.

The other type of mixing is referred to as "transport-controlled." The mixed material is entrained in the adjacent layers at a rate which is greater than the rate of exchange. The two-layered system continues to exist and the mass exchanged through the interface is rapidly transported into the adjacent layers. The overall properties--e.g., temperature--of these layers gradually change as a result, but the layers remain homogeneous in cross sections perpendicular to the flow.

It was this latter, "transport-controlled" type of mixing process which occurred at greater distance from the warm water outlet in the flume experiments. No permanent intermediate layer formed. A "mixing wedge" near the outlet could be observed in the the case of the submerged hydraulic jump, but at greater distances the rate of mixing within layers was higher than the rate of exchange across the interface. One might speculate that a flow cannot mix more fluid than it can actually entrain under steady conditions if there is no local additional energy input. There is no evidence that this is true, but one could argue that the turbulence or energy which produces the mixing comes from the interior of the fluid and that the turbulence level or main transport capacity at the interior of the layer must be larger than near the interface where it is damped. The formation of an intermediate layer would then require external energy input.

Heat is transported from the warmer portion of the fluid to the colder one by convection or conduction, and heat flow cannot be separated from mass flow. The contribution of conductive heat transport in laboratory experiments can be substantial.

In the flume experiments there is some heat loss through the water surface and the walls of the flume. Consequently, the total heat flux in the general flow direction will decrease with distance from the outlet.

Examples of the temperature patterns along the flume which are associated with different types of flow are shown in Fig. 9. It can be seen that under certain circumstances violent mixing near the outlet may occur. But in at least part of the flow region the flow can be considered essentially horizontal.

Under steady conditions velocity and temperature distributions are time-independent. A steady state can be obtained only if colder water is constantly added to the flume to compensate for cold water losses by entrainment or conductive heating. Through flow of cold water at a rate equal to or larger than the amount lost is therefore essential in all experiments carried out in flumes and tanks which do not permit complete regeneration of cold water by cooling of the warm water discharge. A small enough cold water flow rate was chosen that the velocity pattern which it generated did not substantially interfere with the flow pattern to be studied. Inflow and outflow at a deep point in the reservoir and small discharge velocities are likely to produce the least interference. If the experimental flume is terminated by a single weir over which both warm and cold water leave the experimental facility, the effect of the cold water flow on the position of the interface must be considered important.

APPENDIX D

THOUGHTS ON THE TWO-DIMENSIONAL BUOYANT JET AND THE INTERNAL HYDRAULIC JUMP

The internal hydraulic jump at the interface of two horizontal layers of slightly different density was analyzed by Yih [7] by analogy with open channel flow. Mixing and friction at the interface and in the jump were ignored. The results of the analysis may be applied to the cooling water outlet. Caution is necessary, however, not only because of the above assumptions, but also because the flow at the outlet is a flow confined between a free surface and a solid bottom and does not have a free interface. As seen from Fig. 4, an internal hydraulic jump can form only if the internal Froude number at the outlet is larger than a critical value which is close to 1.4. Whether the internal jump will be free or submerged will then depend on the position of the tailgate. If applicable, the above-mentioned analysis holds only for the free internal jump because of the assumptions made.

In the two-dimensional flume experiments it was difficult to identify an internal hydraulic jump and, in particular, the conjugate depths. This was because the layer of warm water begins to spread as a two-dimensional jet as soon as it leaves the outlet due to entrainment of neighboring fluid. There is eventually a transition into an internal hydraulic jump which is thought to be characterized by a reversed current. In regular open-channel flow with a free surface air is entrained, but this does not obscure the free surface.

The impulse-momentum principle can be applied to both the jet and the hydraulic jump, the only difference being that gravity forces are taken into account for the hydraulic jump analysis but not for the jet. This is only a very minor difference, however, because gravity forces in the stratified system are very small when compared to inertial forces.

The conjugate depths of a free hydraulic jump in open-channel flow are found at the beginning and end of the hydraulic jump. The same applies to the free internal hydraulic jump. To find the conjugate depths experimentally it is therefore necessary to define and locate the beginning and end of the jump, which proves to be difficult.

Downstream from the hydraulic jump the gradient of the thickness of the warm water layer is very small, and it seems fairly well justified by the present experiments in a long flume to choose the largest depth downstream from the internal hydraulic jump as one of the conjugate depths.

At the upstream end the situation is more complex. Observation of the interface and the mixing processes alone does not yield any clear information on the actual length of the internal hydraulic jump.

It appears desirable to use the velocity distribution to resolve these difficulties. Within a regular hydraulic jump, flow is partially reversed and the upstream end of the hydraulic jump coincides with the first appearance of negative flow velocities. If the velocity distribution within an internal hydraulic jump is studied, an analogous point can be found and used as the upstream end of the hydraulic jump. Theoretically, this point must coincide with the outlet bottom if the outlet depth, d_o, is to be the upstream conjugate depth. Figure 16 represents the internal hydraulic jump schematically.

Another, and probably the easiest, method of defininining the upstream conjugate depth is a visualization technique whereby dye is added to the flow downstream from the hydraulic jump. It can then be observed how far upstream the dye is carried. If dilution is not excessive the location of the upstream conjugate depth can thus be found.

Special conditions exist if the outlet flow is laminar and supercritical. There is no flow reversal in the upper layer. The interface is either completely smooth or undular. Eventually interfacial breaking waves will occur. The outlet flow in this case is a laminar, two-dimensional, buoyant jet.

In a non-buoyant jet of the same kind the velocity component in the x-direction, according to Schlichting [11], is

$$u = 0.4543 \left(\frac{K}{\nu x}\right)^{1/3} (1 - \tanh^2 \xi)$$

where

$$\xi = 0.2752 \left(\frac{K}{\nu^2}\right)^{1/3} \frac{z}{x^{2/3}}$$

The centerline velocity is obtained for $z = 0$. The location of all points of which the x component of the velocity is a fraction ε of the centerline velocity can be found from the relationship

$$\mathcal{E} = \frac{u(x_1 z)}{u(x_1 0)} = 1 - \tanh^2 \xi$$

or

$$0.2752 \left(\frac{K}{\nu^2}\right)^{1/3} \frac{z}{x^{2/3}} = \text{arc tanh } (1 - \mathcal{E})^{1/2}$$

A spreading angle may then be defined as

$$\text{tg } \beta = \frac{z}{x} = \frac{\text{arc tanh}(1 - \mathcal{E})^{1/2}}{0.2752(Kx/\nu^2)^{1/3}}$$

Applied to one particular experiment in which $\mathcal{E} = 0.05$, $Q_o = 0.001$ cfs, $d_o = 0.05$ ft, and $u_o = 0.5$ ft, the limit of the two-dimensional laminar jet is found to be

$$z = 0.0184\, x^{2/3}$$

A comparison of this result with measurements for the actually buoyant jet shows the effect of buoyancy on the spreading of the jet quite clearly (Fig. 17).